Interpretive Summary

Prepartal high-energy feeding with grass silage-based diets does not disturb the hepatic adaptation of dairy cows during the periparturient period

Qin, N.

The effects of prepartal energy level on hepatic lipidome and transcriptome of dairy cows during the periparturient period were studied. Prepartal high-energy feeding elevated hepatic sphingolipid levels and downregulated hepatic inflammatory and acute phase responses one week prior to parturition. There was no evidence indicating that prepartal high-energy feeding disturbed hepatic adaptation. The findings will provide the basis of guidelines for nutritional management prepartum that will improve health and welfare in dairy cows during the periparturient period.

12 **OVERFEEDING DOES NOT DISTURB LIVER ADAPTATION**

13 **Prepartal high-energy feeding with grass silage-based diets does not disturb the hepatic**
14 **adaptation of dairy cows during the periparturient period**

15 **Nanbing Qin*, Tuomo Kokkonen*, Siru Salin*, Tuulikki Seppänen-Laakso†, Juhani**
16 **Taponen‡, AilaVanhatalo* and Kari Elo*[1]**

17 *Department of Agricultural Sciences, P.O. Box 28, FI-00014 University of Helsinki, Finland
18 †Industrial Biotechnology, VTT Technical Research Centre of Finland Ltd, Tietotie 2, P.O. Box
19 1000, FI-02044 VTT, Finland
20 ‡Department of Production Animal Medicine, University of Helsinki, Paroninkuja 20, FI-04920,
21 Saarentaus, Finland
22 [1]Corresponding author: kari.elo@helsinki.fi
23

ABSTRACT

The liver of dairy cow naturally undergoes metabolic adaptation during the periparturient period in response to the increasing demand for nutrients. The hepatic adaptation is affected by prepartal energy intake level and is potentially associated with inflammatory responses. To study the changes in the liver function during the periparturient period, 16 cows (body condition score: 3.7 ± 0.3, mean ± SD; parity: second through fourth) were allocated to a grass silage-based controlled-energy diet (104 MJ/day) or a high-energy diet (135 MJ/day) during the last 6 wk before the predicted parturition. Liver samples were collected by biopsy at 8 d prior to the predicted parturition (-8 d) and at 1 and 9 d after the actual parturition (1 d and 9 d). The lipidomic profile of liver samples collected at -8 and 9 d was analyzed using ultra performance liquid chromatography-mass spectrometry-based lipidomics. Liver samples from all the time points were subjected to microarray analysis and the subsequent pathway analysis with Ingenuity Pathway Analysis software. Prepartal energy intake level affected hepatic gene expression and lipidomic profiles prepartum, while little or no effect was observed postpartum. At -8 d, hepatic lipogenesis was promoted by prepartal high-energy feeding through the activation of *X receptor*/*retinoid X receptor* pathway and through increased transcription of *thyroid hormone-responsive* (*THRSP*). Hepatic inflammatory and acute phase responses at -8 d were suppressed (z-score = -2.236) by prepartal high-energy feeding through the increase in the mRNA abundance of *suppressor of cytokine signaling 3* (*SOCS3*) and the decrease in the mRNA abundance of *interleukin 1* (*IL1*), *nuclear factor kappa B 1* (*NFKB*), *apolipoprotein A1* (*APOA1*), *serum amyloid A3* (*SAA3*), *haptoglobin* (*HP*), *lipopolysaccharide binding protein* (*LBP*), and *inter-alpha-trypsin inhibitor heavy chain 3* (*ITIH3*). Moreover, prepartal high-energy feeding elevated hepatic concentrations of C18- (7%), C20- (17%), C21- (26%), C23-sphingomyelins (26%), and total saturated sphingomyelin (21%). In addition, cows in both groups displayed increased lipogenesis at gene expression level after parturition and alterations in the concentration of various sphingolipids between the first and last samplings. In conclusion, prepartal high-energy feeding promoted

lipogenesis and suppressed inflammatory and acute phase responses in the liver before parturition, while only minor effects were observed after parturition.

KEYWORDS: dairy cow, periparturient period, physiological adaptation, microarray, lipidomic profiling

INTRODUCTION

Dairy cows undergo a series of physiological adaptations during the periparturient period due to the increasing energy requirement and the subsequent negative energy balance. The physiological adaptations are partly mediated by insulin resistance (**IR**) and the change in plasma insulin concentration (Bell and Bauman, 1997). These changes lead to the mobilization of body reserves to the tissues in demand (Bell, 1995; Vernon, 2005). A part of mobilized nutrients are allocated to the liver, where they induce hepatic adaptation, including increased gluconeogenesis and ketogenesis (Aiello et al., 1984; Herdt, 2000). Hepatic adaptation is regulated at gene expression level as altered mRNA abundance near calving was observed in genes involved in various metabolic pathways (Loor et al., 2005; McCarthy et al., 2010). In addition, hepatic adaptation is potentially associated with the inflammatory status as negative energy balance is accompanied by increased inflammation induced by pro-inflammatory cytokines (Trevisi et al., 2012), which stimulate hepatic synthesis and secretion of positive acute phase proteins (Bionaz et al., 2007).

Hepatic adaptation is potentially affected by prepartal energy intake level of cows. Prepartal high-energy feeding has been reported to exacerbate the lipid mobilization from AT, particularly after parturition, as characterized by the elevated plasma non-esterified fatty acid (**NEFA**) level (Douglas et al., 2006; Janovick et al., 2011), and evidenced by the decreased expression of lipogenic genes in AT (Selim et al., 2015). As a consequence, the liver may be supplied with the excessive abundance of NEFA, which promotes hepatic lipogenesis and may lead to various metabolic disorders (Ingvartsen, 2006; Loor et al., 2006). Moreover, excessive energy intake prepartum and increased visceral adiposity may predispose dairy cows to inflammation and impaired liver function (Loor et al., 2006). In human and mice, inflammation is considered as a mechanism that induces IR (McArdle et al., 2013). However, there are controversial reports whether prepartal high-energy feeding (Mann et al., 2016; Salin et al., 2017) or increased adiposity (Shahzad et al., 2014; De Koster et al., 2015) leads to increased systemic IR in periparturient cows.

Sphingolipids are a class of lipids closely associated with the glucose homeostasis in human and mice (Larsen and Tennagels, 2014). Ceramides (**Cer**), the most abundant sphingolipids in the cell, have been recognized to trigger IR and their production is influenced by the inflammatory response (Chavez and Summers, 2012). In recent years, the application of lipidomics has enabled novel insights into the role of sphingolipids in the physiological adaptation in periparturient cows. Changed sphingolipid concentrations near calving were reported in the plasma, liver, AT, and skeletal muscle of cows (Imhasly et al., 2015; Qin et al., 2017; Rico et al., 2017). Comparisons between cows of different adiposity further suggested the associations between lipid mobilization and the concentrations of Cer, hexosyl ceramide (**HexCer**), and lactosylceramide in plasma and liver and the association between systemic IR and specific Cers during the periparturient period (Rico et al., 2015, 2017). Moreover, prepartal high-energy feeding was reported to increase the concentration of specific Cers and the total concentration of sphingomyelin (**SM**) in AT near calving (Qin et al., 2017).

We aimed to study effects of prepartal energy level on the hepatic adaptation of dairy cows during the periparturient period through the parallel analyses on global gene expression and lipidomic profiles. Firstly, we hypothesized that prepartal high-energy feeding increases hepatic lipogenesis. Secondly, we hypothesized that prepartal high-energy feeding increases hepatic Cer concentrations and upregulates genes related to inflammation during the periparturient period.

MATERIALS AND METHODS

Animals, Diets, Samplings, and Glucose Tolerance Tests

The feeding experiment, feed composition, and collection of biopsies were described in detail in Selim et al. (2014). Sixteen Finnish *Ayrshire* dairy cows were involved in the feeding experiment in a randomized complete-block design. The cows were paired according to parity (second through fourth), body weight (693 ± 57 kg, mean ± SD), and body condition score (**BCS;** 3.7 ± 0.3, mean ± SD). The two cows in each pair were randomly allocated to two dietary treatment groups on 44 ± 5 d

(mean ± SD) prior to the actual parturition date. The grass silage-based dietary treatments included a controlled-energy (**CON**) diet (100% of the energy requirement of pregnant dairy cow; Luke, 2018) and a high-energy (**HIGH**) diet targeting to meet 150% of the energy requirement of a pregnant cow. In the ad libitum-fed HIGH group, the actual average energy intake was 144% of the energy requirement of pregnant dairy cow during the first 3 wk of experimental feeding. During the last 3 wk before the predicted parturition, the energy allowance of the HIGH group was decreased by 5% on alternate days by gradually restricting DMI as described in more detail by Salin et al. (2017). The average ME was 99 MJ/d in the CON group and 141 MJ/d in the HIGH group from wk 6 to wk 4 prepartum and 109 MJ/d in the CON group and 128 MJ/d in the HIGH group from wk 3 to wk 1 prepartum. After parturition, all cows were fed wilted grass silage ad libitum, supplemented with increasing amount of small grain-based concentrate, starting from 5 kg/d on the day of parturition and increasing to 9 kg/d at 9 d postpartum (average ME 11 MJ/d during the first 2 weeks of lactation). The liver samples were collected by biopsy 8 d prior to the predicted parturition (11 ± 5 d in the actual operation) and 1 and 9 (± 1) d postpartum (the three time points are hereafter represented as **-8 d**, **1 d**, and **9 d**). Lipidomic and microarray analyses were conducted on 22 and 32 biopsy samples, respectively. The selection of samples was at random in respect of pairs to represent the design of the whole study. Intravenous glucose tolerance tests (**IVGTT**) were performed on the cows 10 ± 5 d (mean ± SD) prior to the actual parturition and 10 ± 1 d (mean ± SD) postpartum and the results have been published by Salin et al. (2017). The basal NEFA concentrations at 10 ± 5 d (mean ± SD) prior to the parturition and 10 ± 1 d postpartum were calculated by averaging the measurements on the blood samples collected 15 and 5 min before the IVGTT (Salin et al., 2017).

Lipidomic Profiling

Liver biopsies were pulverized using Covaris CryoPrep (Covaris Inc., Woburn, MA, USA) and an internal standard mixture containing examples of major lipid classes as esters with C17:0 fatty acid was added to the weighed aliquots of samples. Lipids were extracted (chloroform: methanol 2:1) with

Retsch Mixer Mill homogenizer (Retsch Gmbh, Haan, Germany). After extraction, a mixture containing three labeled standards was added in order to control the extraction process. The whole-lipidome analyses were performed with a Waters quadrupole time-of-flight Premier mass spectrometer combined with an Acquity Ultra Performance LC™ (Waters Corp., Milford, MA, USA) by using an Acquity UPLC™ BEH C18 column (2.1 × 100 mm with 1.7 μm particles). The solvent system consisted of ultrapure water (1% 1 M NH4Ac, 0.1% HCOOH) and a mixture of acetonitrile: isopropanol (1:1, 1% 1M NH4Ac, 0.1% HCOOH). All solvents used were liquid chromatography-mass spectrometry grade, and reference lipids were obtained from Avanti Polar Lipids, Inc. (Alabaster, AL, USA) and Larodan Fine Chemicals AB (Solna, Sweden). Quantification of all Cer, HexCer, and SM subspecies was based on the comparison with peak heights of internal standard Cer (d18:1/17:0).

The data processing using MZmine 2 software included alignment of peaks, peak integration, normalization, and peak identification based on an internal spectral library. The analytical procedure was modified from that in Nygren et al. (2011), as described by Qin et al. (2017). The profiling of Cer and HexCer was carried out, using the negative-electrospray ionization mode, and the profiling of SM was carried out, using the positive-electrospray ionization mode. In total, 26 Cers, 6 HexCers, and 9 SMs were identified and quantified (μmol/g wet tissue) in the liver biopsies.

Microarray Analysis

Liver samples collected with biopsy were stored in a protective solution (Allprotect Tissue Reagent; Qiagen GmbH, Hilden, Germany) at -20 °C before total RNA extraction. Approximately 3-5 mg of liver was homogenized, using a TissueRuptor homogenizer (Qiagen). Total RNA was extracted with an RNeasy Mini Kit (Qiagen) according to the manufacturer's instruction.

Quantification of total RNA was performed with a NanoDrop 1000 spectrophotometer (ThermoFisher Scientific, Waltham, MA, USA). The quality of the RNA samples was assessed, using

an Agilent Bioanalyzer 2100 chip electrophoresis system and Agilent RNA 6000 Nano Kit (Agilent Technologies, Santa Clara, CA, USA).

A total of 32 liver RNA samples were analyzed, using Affymetrix GeneChip® Bovine Genome Arrays (Affymetrix Inc., Santa Clara, CA, USA), including five, six, and six samples from the CON group and five, four, and six samples from the HIGH group at -8, 1, and 9 d, respectively. The arrays contained 24,027 probe sets, representing more than 23,000 transcripts. All RNA samples used in the array analyses showed RNA integrity number values higher than 8.9, and a total of 100 ng of RNA were used per array. All RNA samples and arrays were preprocessed, hybridized, and scanned by Biomedicum Genomics at the University of Helsinki.

Since the amount of genomic sequence information has increased, the original annotations for the Affymetrix arrays were based on incomplete information. The annotations were supplemented by interrogating sequence databases and taking into account recent information (Cow Ensembl release 86; National Center for Biotechnology Information (NCBI) *Bos taurus* Annotation Release 105).

Calculations and Statistical Analyses

The sphingolipid subspecies were further sorted and the concentrations were summed up, according to their fatty acid or sphingosine composition. The concentration of sphingolipids and further-sorted sphingolipid subclasses was log-2 transformed to normalize the data. The transformed data were imported into SAS (release 9.3; SAS Institute, Cary, NC, USA) for statistical analyses. The normality of residuals of the transformed data was tested with PROC MIXED and PROC UNIVARIATE procedures, using a model including diet as a fixed effect and pair as a random effect. The repeated-measures ANOVA was performed using PROC MIXED procedure, in which treatment, time, and their interaction were set as fixed effects, pair and the interaction between pair and time were set as random effects, and animal was set as a within-subject effect. Three covariance structures were applied in the analyses, including compound symmetry (CS), unstructured (UN), and spatial power

(SP) law (POW). The structure giving the smallest Bayesian information criterion was eventually selected. The SLICE option of the PROC MIXED procedure was used to test the effect of diet within each time point. *P*-values lower than 0.05 were considered significant and those of $0.05 < P < 0.10$ represented tendencies toward significance. Heatmaps were composed based on the original concentration of all sphingolipid subspecies with MetaboAnalyst 3.0 (http://www.metaboanalyst.ca/, Xia Lab, McGill University; Xia et al., 2015). Spearman correlation analyses were performed between hepatic lipid concentrations, and the relative expression levels of selected hepatic genes obtained from the microarray analysis or the previous quantitative PCR (**qPCR**) analyses (Selim et al., 2014) and parameters from IVGTT (Salin et al., 2017) using PROC CORR procedure.

The analysis of microarray data, including quality control, preprocessing, normalization, and statistical analysis, was carried out using R (https://www.r-project.org/), Bioconductor (https://www.bioconductor.org/), and Chipster software package (v. 3.9, CSC-IT Center for Science Ltd, Finland; Kallio et al., 2011). With Simpleaffy package in R software, a plot of quality-control metrics was performed for all 32 arrays to test the comparability of the scaling factors. Using Chipster software, we prepared an RNA degradation plot of all the arrays and spike-in-performance log-log plots of the signal intensity versus the RNA concentration for all 32 microarrays to further analyze the quality of the array hybridizations. The normalization was performed using the robust multiarray average method (Irizarry et al., 2003). The quality of the normalized data was evaluated with the box plots of the relative log expression and normalized unscaled standard error in Chipster. The variance in gene expression between the HIGH and CON groups was analyzed, using the local-pooled-error (LPE) test within the three time points (Jain et al., 2003). A false discovery rate control was performed on the *P*-values obtained, based on the method described by Benjamini and Hochberg (2000), generating a new dataset of adjusted *P*-values. The genes with adjusted-$P < 0.05$ were defined as the differentially expressed genes (**DEG**) between the two groups. The variance in gene expression over time was analyzed between all the time points (-8 vs. 1 d, 1 vs. 9 d, and -8 vs. 9 d), using the linear

model in Chipster, involving diet and time as the main effects after pairing the data from the same cow, followed by the same false-discovery rate control described above. Genes with adjusted-$P < 0.05$ were considered to have different transcription levels between time points. The microarray data are available at the Gene Expression Omnibus page (https://www.ncbi.nlm.nih.gov/geo/) under accession number GSE97437.

The microarray data were further analyzed with Ingenuity Pathway Analysis (**IPA**) System (v. 7.5; Ingenuity Systems, Mountain View, CA, USA; http://www.ingenuity.com). The input of the pathway analyses included DEGs identified in the microarray analysis and those identified in the previous qPCR with the analysis of variance between the CON and HIGH groups at all three time points (Selim et al., 2014). A dataset of DEGs, containing their gene symbols, *P*-values, and the log ratios of their expression in the HIGH group to that in the CON group, was imported into IPA. The genes in the dataset were mapped in IPA according to their gene symbols based on Ingenuity human and rodent knowledge base. The DEGs were grouped into canonical pathways, functions, and diseases, based on the right-tailed Fisher Exact Test, which is a measurement of the likelihood that the association between a set of DEGs in the experiment and a given process or pathway is due to random chance. Networks of the DEGs were composed, based on the connection between genes, as referenced from previous literature in the knowledge base. The networks were ranked according to their scores, calculated from the number of network eligible DEGs in one network, the total number of network eligible DEGs in the whole analysis, and the total number of molecules that potentially make up this network based on the knowledge base (Jiménez-Marín et al., 2009).

RESULTS

Sphingolipid Profiles in the Liver

The most abundant Cer subspecies in the liver at -8 and 9 d were Cer (24:0), Cer (23:0), and Cer (22:0), taking up 23.6%, 21.3%, and 17.8% of the total Cer, respectively. Cer subspecies containing

an SFA comprised 86.7% of the total Cer, with the remainder containing a MUFA. From the aspect of sphingosine profiles, Cer (d18:1) represented 89.9% of the total Cer in the liver. Among SM, C16- and C23-SM were the top two abundant subclasses in the liver, comprising 43.0% and 31.4% of the total SM in concentration. Eighty-five percent of the SM contained an SFA, with those containing a MUFA forming the rest.

The heatmap showed that higher level of sphingolipids tended to appear in the liver of the HIGH group than in the CON group at -8 d (Figure 1). In contrast, the difference in sphingolipid concentrations between the groups was much less apparent at 9 d. The further statistical analyses on sorted sphingolipid subclasses showed that the concentrations of Cer (23:0) ($P = 0.088$), Cer (23:1) ($P = 0.099$), Cer (24:1) ($P = 0.080$), and Cer (25:1) ($P = 0.052$) tended to be higher in the HIGH group compared with the CON group (Table 1). The comparison within time points showed that the different levels of Cer (24:1) ($P = 0.020$) and Cer (25:1) ($P = 0.019$) between groups were mainly contributed by the difference in their prepartal concentrations. None of the Cer subspecies differed in concentration after parturition. The majority of Cer subspecies displaying different concentrations between groups were MUFA-Cer, which is also shown by the tendency towards higher ($P = 0.081$) total MUFA-Cer concentration in the HIGH group than in the CON group (Table 1). In addition, prepartal high-energy feeding elevated the concentrations of C18- ($P = 0.007$), C20- ($P = 0.004$), C21- ($P = 0.035$), and C23-SM ($P < 0.001$), and the total concentration of saturated SM ($P = 0.004$) in the HIGH group compared with the CON group (Table 1). Similarly to Cers, the comparison within time points showed that the significant effect of prepartal high-energy feeding on SMs was mainly derived prepartum.

Considering the change of sphingolipids in the liver over time regardless of the diet, the heatmap showed that the concentration of most HexCer and SM subspecies decreased from -8 to 9 d, with HexCer (d18:1/23:0), HexCer (d18:1/22:0), SM (d18:1/20:0), and SM (d18:1/21:0) being the exceptions (Figure 1). The patterns in Cer concentrations over time varied with the length of their

acyl chains. Moreover, the number of double-bonds in the acyl chain and the sphingosine type also influenced the patterns in Cer concentrations over time. For instance, we observed contrasting patterns over time between Cer (d18:1/20:0) and Cer (d18:2/20:0) and between Cer (d18:1/24:0) and Cer (d18:1/24:1). The further statistical analyses showed significant declines over time in a number of Cer subclasses, including Cer (18:0) ($P = 0.042$), Cer (23:1) ($P = 0.014$), Cer (25:1) ($P = 0.025$), Cer (26:0) ($P < 0.001$), and Cer (26:1) ($P < 0.001$; Supplemental Table S1). Exceptionally, an increase ($P = 0.030$) from -8 to 9 d was observed in Cer (23:0). From the aspect of sphingosine profiles, we observed significant increases in Cer (d17:1) ($P = 0.044$) and Cer (d18:0) ($P = 0.014$) concentrations whereas a decrease ($P < 0.001$) in Cer (d18:2) concentration from -8 to 9 d was observed (Supplemental Table S1). In addition, significant decreases over time were observed in various SM subclasses, including C16- ($P = 0.037$), C18- ($P = 0.011$), C24- ($P = 0.036$), and MUFA-SM ($P = 0.002$).

Pathway Analyses on DEGs between the Feeding Groups

In the microarray analysis, we identified 106, 67, and 52 DEGs between the two groups at -8, 1, and 9 d, respectively. Subsequently, IPA software successfully mapped 74 genes at -8 d, 43 genes at 1 d, and 36 genes at 9 d (Supplemental Table S2) and grouped these genes into pathways, functions, and diseases (Table 2). We identified 57, 52, and 29 pathways with $P < 0.05$ at -8, 1, and 9 d, respectively, in the canonical pathway analyses in IPA. Of these, only two pathways at -8 d displayed significant difference between the HIGH and CON group based on the calculation of z-score (Supplemental Figure S1), i.e. the downregulation of acute phase response signaling (z-score = -2.236; $P < 0.0001$; Supplemental Figure S2) and the upregulation of *liver X receptor*/*retinoid X receptor* (***LXR/RXR***) activation (z-score = 0.816; $P < 0.0001$; Supplemental Figure S3). The downregulation of acute phase response signaling was characterized by the upregulated transcription of *suppressor of cytokine signaling 3* (***SOCS3***) and the downregulated transcription of *interleukin 1* (***IL1***), *nuclear factor kappa B 1* (***NFKB1***), *apolipoprotein A1* (***APOA1***), *serum amyloid A3* (***SAA3***), *haptoglobin* (***HP***),

lipopolysaccharide binding protein (***LBP***), and *inter-alpha-trypsin inhibitor heavy chain 3* (***ITIH3***). The upregulation of *LXR/RXR* activation pathway was characterized by the upregulated transcription of *apolipoprotein A4* (***APOA4***) and the downregulated transcription of *APOA1*, *IL1*, *LBP*, and *NFKB1*. In contrast, we observed no significant pattern in pathways at 1 and 9 d. In the network analyses, we identified two gene networks containing more than 20 DEGs, i.e. lipid metabolism, small-molecule biochemistry, and vitamin and mineral metabolism (score 51, 22 focus molecules) at -8 d and connective-tissue disorders, inflammatory disease, and skeletal and muscular disorders (score 53, 20 focus molecules) at 9 d. The network identified at -8 d displayed the association between the DEGs in the significant canonical pathways and other DEGs (Supplemental Figure S4).

Changes in Gene Expression over Time

We observed that 158 genes were differentially expressed for 1 d vs. -8 d. The numbers were 383 for 9 d vs. 1 d and 654 for 9 d vs. -8 d (adjusted $P < 0.05$). The DEGs between time points involved in inflammatory response, acute phase response, sphingolipid metabolism, and lipogenesis were presented (Figure 2 and Figure 3).

Correlation Analyses

We observed negative correlations between BCS at 2 wk prepartum and the hepatic concentration of various Cer subclasses at -8 d, including Cer (18:0) (r = -0.79; $P = 0.001$), Cer (19:0) (r = -0.60; $P = 0.030$), Cer (24:0) (r = -0.66; $P = 0.014$), Cer (25:1) (r = -0.60; $P = 0.029$), Cer (26:0) (r = -0.66; $P = 0.014$), and Cer (26:1) (r = -0.77; $P = 0.002$). In addition, plasma NEFA concentration was negatively correlated with various Cer subclasses, e.g., Cer (18:0) prepartum (r = -0.63; $P = 0.039$) and Cer (16:0) postpartum (r = -0.77; $P = 0.005$). Glucose area under curve in IVGTT postpartum was negatively correlated with hepatic concentration of various Cer subspecies at 9 d, including Cer (18:0) (r = -0.64; $P = 0.035$), Cer (23:0) (r = -0.65; $P = 0.029$), Cer (24:0) (r = -0.80; $P = 0.003$) and Cer (25:0) (r = -0.72; $P = 0.013$). The relative expression level of *SAA3* in microarray was negatively

299 correlated with hepatic C18-SM concentration at -8 d (r = -0.71; *P* = 0.047). The relative expression
300 level of *LBP* in microarray was negatively correlated with hepatic concentrations of C16- (r = -0.74;
301 *P* = 0.037) and C18-SM (r = -0.90; *P* = 0.002) at -8 d. The relative expression level of *IL1A* in
302 microarray was negatively correlated with hepatic C20-SM concentration (r = -0.76; *P* = 0.028) at -
303 8 d.

304 **DISCUSSION**

305 This study presents the changes in hepatic lipidomic and gene expression profiles during the
306 periparturient period in response to different prepartal energy intake levels. Parts of the results from
307 the same experiment were published in earlier papers, including the whole-lipidome analyses in the
308 liver and AT (Qin et al., 2017), the IVGTT results (Salin et al., 2017), the measurements of animal
309 performance and blood metabolites, and the qPCR analyses of seven hepatic genes involved in insulin
310 signaling, inflammatory response, and gluconeogenesis (Selim et al., 2014). Despite the marked
311 difference in energy intake between the two feeding groups, we found no diet effect in either BW
312 change (1.3 vs. 1.1 kg/d; HIGH vs. CON) during the dry period or BCS before calving (3.7 vs. 3.8;
313 HIGH vs. CON). However, we observed that the HIGH had lower basal blood NEFA concentration
314 than the CON group in IVGTT at 1 wk prior to parturition (Salin et al., 2017). In contrast, the basal
315 NEFA levels after parturition were not different between the feeding groups (Salin et al., 2017). In
316 addition, results from IVGTT suggested little or no difference in whole-body insulin sensitivity
317 between the HIGH and CON group at1 wk prior to parturition to 1 wk postpartum (Salin et al., 2017).
318 Analogous to our previous results, the present results showed a greater effect of prepartal energy level
319 on both the lipidomic and gene expression profiles before parturition than after.

320 ***Hepatic lipogenesis***

321 Previously we reported that the HIGH group had higher hepatic total lipid concentration compared
322 with the CON group at -8 and 9 d (Qin et al., 2017). At the gene expression level, the increase of total

lipid concentration under prepartal high-energy feeding was reflected by the upregulation of *LXR/RXR* activation pathway in the HIGH group compared with the CON group at -8 d because *LXR/RXR* activation is a pathway that promotes lipogenesis by stimulating sterol regulatory element-binding protein 1c (Schultz et al., 2000). However, we observed no differential expression in the single genes of nuclear receptors *LXR* and *RXR* between groups, although the pathway was identified as significantly upregulated in the canonical pathway analysis. The increase in lipogenesis was supported by the upregulation of *thyroid hormone-responsive* (***THRSP***) in the HIGH group compared with the CON group at the same time point (Supplemental Figure S4). The gene *THRSP* promotes hepatic lipogenesis, and its expression is regulated by *LXRα* through a sterol regulatory element-binding protein 1c-dependent mechanism in mice (Wu et al., 2013). The lipogenic role of *THRSP* was previously reported in the mammary epithelial cell of ruminants (Cui et al., 2015; Yao et al., 2016). Previously, Khan et al. (2014) reported that high-energy feeding during the entire dry period increased hepatic transcription of various lipogenic genes before parturition, including *THRSP*. However, the difference in the feeding approaches between our study and Khan et al. (2014) may decrease the comparability between results. We gradually reduced the energy allowance in the HIGH group during the close-up period. This was not applied in Khan et al. (2014), although they observed a gradual decrease in DMI when approaching calving. Earlier studies have shown that the high energy intake during the far-off dry period is often associated with a decline of DMI during the close-up dry period and the decline has been up to 30% in corn silage-based diet (Grummer et al., 2004). This has led to the decreased difference in energy balance between the treatments with ad libitum and the controlled-energy feeding (Dann et al. 2006). Based on these findings, we manipulated the feed intake in the HIGH group by decreasing the energy allowance by 5% on alternate days through the gradual restriction of DMI during the last 3 wk before parturition (Salin et al., 2017), in order to test whether the high-energy feeding during the early dry period accompanied by a large decline of feed intake during the close-up dry period is detrimental to the physiological adaptation of dairy cows in grass

348 silage-based feeding. It is worth noting that the high-energy feeding still increased the average energy
349 allowance by 30% compared with the control during the whole experimental period (135 MJ/day vs.
350 104 MJ/day). Indeed, Dann et al. (2006) reported that the high-energy feeding during the far-off dry
351 period had significant negative effects on the periparturient metabolism of dairy cows, whereas no
352 effect was observed for the high-energy feeding during the close-up dry period. In the present study,
353 the difference in energy intake between the HIGH (140% of CON during wk 6 and 4 prior to
354 parturition) and CON group was profound during the far-off dry period. Therefore, we consider that
355 it is profitable to compare our results with other high-energy feeding studies.

356 As reported in our earlier publication, the HIGH group had lower plasma NEFA concentration
357 prepartum compared with the CON group. Despite the decrease in plasma NEFA, the HIGH group
358 displayed upregulated hepatic lipogenesis before parturition, based on the results from the microarray
359 analysis. In the previous qPCR analyses on the same animals, we observed potentially suppressed
360 fatty acid oxidation in the liver of the HIGH group compared with the CON group, based on the
361 expression profile of *carnitine palmitoyltransferase 1A* (***CPT1A***; Selim et al. 2014), which encodes
362 the CPT1 enzyme that facilitates the entry of fatty acids into mitochondria (Drackley et al., 2001).
363 We suggest that the suppressed fatty acid oxidation under high-energy feeding may have outweighed
364 the decrease in hepatic NEFA uptake and thus may have compensated for the lower influx of fatty
365 acids in the liver, ultimately leading to the net increase in hepatic lipogenesis in the HIGH group
366 compared with the CON group before parturition. The corresponding result was reported by Loor et
367 al. (2006) showing that overfed cows had lower plasma NEFA levels and lower expression of genes
368 related to hepatic fatty acid oxidation prepartum compared with cows in a restricted-energy diet.

369 The stimulation of lipogenic pathways by the prepartal high-energy feeding disappeared after
370 parturition. Moreover, the cows in the HIGH diet showed no greater lipid accumulation in the liver
371 than did the cows in the CON diet after parturition (Qin et al., 2017). However, regardless of the diet,
372 the cows displayed the accumulation of lipid in the liver after parturition, as suggested by the dramatic

increases in the concentration of triacylglycerol (**TAG**) and its precursor diacylglycerol (**DAG**) from -8 to 9 d (Qin et al., 2017). The lipid accumulation was reflected by the expression profiles of various lipogenic genes over time (Figure 3). The transcription of fatty acid transporters, including *fatty acid binding protein 4* (***FABP4***) and *solute carrier family 27 member A2* (***SLC27A2***), increased from 1 to 9 d, suggesting a potential increase in hepatic NEFA uptake from the onset of lactation. A similar pattern was previously reported on another fatty acid transporter, showing that hepatic expression of *solute carrier family 27 member A1* (***SLC27A1***) in dairy cows was higher at 1 wk postpartum than at 3 wk prepartum (Gross et al., 2013). Increased NEFA influx after parturition may subsequently stimulate hepatic fatty acid oxidation, reflected by the upregulated hepatic transcription of *carnitine palmitoyltransferase 1B* (***CPT1B***) and *carnitine palmitoyltransferase 1C* (***CPT1C***) from -8 to 9 d. The activation of the CPT1-encoding genes after parturition corresponds to the previous findings of others (Drackley et al., 2005; Akbar et al., 2013; Khan et al., 2014). The transcription of *fatty acid synthase* (***FASN***) and *diacylglycerol O-acyltransferase 2* (***DGAT2***) was higher at 9 d compared with -8 or 1 d, suggesting potentially increased hepatic fatty acid and TAG syntheses after parturition, in line with the finding of Gross et al. (2013), who observed that hepatic *FASN* expression increased dramatically from 3 wk prepartum to 1 wk postpartum. In the liver, TAG is stored as lipid droplets, with perilipins (**PLIN**) forming the surface. We observed higher expression of *PLIN2* and *PLIN3* at 9 d relative to -8 d in both groups, which supports the increased TAG storage as lipid droplets in the liver after parturition and corresponds to the finding of Akbar et al. (2013) showing that hepatic *PLIN2* expression in dairy cows increased from 14 d prepartum to 10 d postpartum. Collectively, the gene expression profiles reflected greater lipid storage and more active lipogenesis in the liver at 1 wk postpartum than at 1 wk prior to parturition.

Hepatic Inflammatory and Acute Phase Responses

Prepartal high-energy feeding downregulated the acute phase response signaling pathway at -8 d based on the gene expression analysis. In cattle, acute phase response proteins have been defined as

indicators of inflammation and fatty liver disease (Nakagawa et al., 1997; Saremi et al., 2013). The downregulation of *SAA3*, *HP*, and *LBP* may reflect a lower grade of inflammation in the liver of the HIGH group than in the CON group at -8 d. This was supported by the downregulation of the pro-inflammatory genes *IL1* and *NFKB1* in the HIGH group compared with the CON group at the same time point, because these genes participate in the mediation of the acute phase response, according to the findings in mice (Bode et al., 2012). Mouse studies have also suggested that SFA and lipopolysaccharides act as potential activators of *toll-like receptor 4* (***TLR4***) and its downstream regulatory gene *NFKB1* (Shi et al., 2006). The gene *NFKB1* can stimulate the production of pro-inflammatory cytokines, including IL1 (Shirasuna et al., 2016). Despite the absence of clear molecular mechanisms, increased expression of the genes encoding pro-inflammatory cytokines and acute phase proteins in the visceral fat was also observed when energy allowance of non-pregnant dairy cows was increased (Ji et al., 2014). Taken together with the lower plasma NEFA concentration compared with the CON group prepartum, we may speculate that the HIGH group had less SFA influx into the liver, leading to a lower grade of inflammation than in the CON group at 1 wk prior to parturition.

Although prepartal high-energy feeding reduced hepatic inflammatory response at -8 d, the difference in inflammatory status disappeared after parturition. Considering the changes over time, we observed that cows in both groups displayed maximal hepatic expression of various cytokine receptors and acute phase proteins at 1 d, including *interleukin 1 receptor type 2* (***IL1R2***), *interleukin 4 receptor* (***IL4R***), *interleukin 10 receptor subunit beta* (***IL10RB***), *SAA3*, *serum amyloid A4* (***SAA4***), *HP*, and *LBP* (Figure 2). The results are in line with the observations by Loor et al. (2005) and Saremi et al. (2012, 2013), suggesting peaked cytokine signaling and acute phase response at parturition due to the systemic inflammation and tissue injury in the uterus. The increase of inflammation at parturition in both groups may have eliminated the difference in the inflammatory response between the two groups after parturition.

Previous findings suggested that high energy intake during the dry period resulted in negative effects on the performance and metabolism of dairy cows after parturition (Dann et al., 2006). However, we observed no impairment in the hepatic metabolism after parturition based on the gene expression profiles, as no pathway was significantly affected by the high-energy feeding at 1 and 9 d. The reason could be that the extent of the high-energy feeding in the present study was insufficient to induce a significant change in the adiposity of cows, as indicated by the similar BCS and systemic insulin sensitivity between the two groups around calving reported in our previous publications (Selim et al., 2014; Salin et al., 2017). The adiposity of cows may act as an important factor that influences the liver function (Roche et al., 2015). Thus, the differences in hepatic metabolism between the groups in the present study may have been limited due to the similar adiposity.

Hepatic Sphingolipid Profile and its Association with Inflammation

The metabolism of Cer is closely associated with inflammation and IR according to the findings in mice (Chavez and Summers, 2012). Recently, associations between plasma and hepatic Cer and HexCer levels and insulin sensitivity were observed in dairy cows after parturition (Rico et al., 2015, 2017). By comparing the Cer profiles between lean and overweight cows, Rico et al. (2017) found that after parturition plasma Cer (16:0) and Cer (24:0) levels were inversely associated with insulin sensitivity. In the present study, we observed negative correlations between BCS at 2 wk prepartum and the concentrations of various Cer subclasses at -8 d, suggesting that before parturition the potentially overweight cows may have lower hepatic Cer levels. Our observation corresponds to the finding of Rico et al. (2017), suggesting that overweight cows tended to have lower levels of Cer (16:0), Cer (24:0), and total Cer in the liver compared with lean cows before parturition.

The concentrations of various SM subclasses were higher in the HIGH group compared with the CON group. SM hydrolysis is catalyzed by acid sphingomyelinase (**ASMase**). The enzyme ASMase was found to be activated in lipopolysaccharide-induced acute inflammation in mice (Wong et al., 2000),

447 and its activation was IL1-dependent (Jenkins et al., 2010). Moreover, a stimulatory effect of SFA on
448 the activity of ASMase was observed in human cells, since it amplified the activation of *TLR4*-
449 induced inflammatory signaling (Jin et al., 2013; Lu et al., 2015). Collectively, the high-energy
450 feeding of dry cows may have suppressed the hepatic inflammatory response through the
451 downregulation of *NFKB1* and *IL1* expression by decreasing the hepatic SFA influx at -8 d, which
452 subsequently reduced ASMase activity. As a consequence, the SM hydrolysis was decreased,
453 resulting in higher hepatic SM concentrations in the HIGH group than in the CON group, as suggested
454 by the negative correlation between *IL1A* expression and hepatic C20-SM concentration. In addition,
455 the negative correlation between *SAA3* expression and C18-SM concentration and that between *LBP*
456 expression and the concentrations of C16- and C18-SM may further support the relationship between
457 inflammation and SM hydrolysis.

458 It is worth noting that negative correlations were also observed between the relative expression level
459 of acute phase proteins (*SAA3* and *LBP*) and the concentrations of several Cer subclasses containing
460 very-long-chain or unsaturated fatty acids (MUFA-Cer, Cer (25:1), and Cer (24:1)), which appeared
461 in higher concentrations in the HIGH group compared with the CON group similarly as SMs.
462 Although there is evidence that several inflammation-related genes are regulated by a mechanism that
463 involves Cer subspecies (Maceyka and Spiegel, 2014), the role of Cer subspecies in the hepatic
464 metabolism is uncertain. The concentrations of total Cer and most Cer subclasses (with Cer (24:1)
465 and Cer (25:1) being the exceptions) were not different between the two groups at -8 d in spite of the
466 potentially lower SM hydrolysis in the HIGH compared with the CON group, suggested by the
467 difference in SM concentrations (Qin et al., 2017). Thus, we suggest that the Cer production may
468 have been supplied through other pathways, including the salvage pathway from other complex
469 sphingolipids and the de novo synthesis from dietary nutrients (Merrill, 2011).

470 In addition to the differences between groups, we observed the time-related differences in hepatic
471 sphingolipid concentration regardless of the diet. The majority of Cer and SM subspecies that varied

over time displayed lower concentrations at 9 d relative to -8 d (Supplemental Table S1). Rico et al. (2017) reported increases in hepatic Cer (24:0) and total Cer concentrations in dairy cows during the periparturient period. However, the increases in Cer concentrations were mainly obvious in the overweight cows but not in lean cows. Rico et al. (2017) grouped the cows based on their BCS while in the present study prepartal high-energy feeding did not affect BCS before calving (Salin et al., 2017), suggesting less difference in the adiposity between groups compared to Rico et al. (2017), which might explain the difference between results.

The changes in sphingolipid concentrations over time were reflected in the expression of *serine palmitoyltransferase small subunit A* (***SPTSSA***) and *serine palmitoyltransferase small subunit B* (***SPTSSB***), which are two genes regulating the rate-limiting enzyme serine palmitoyltransferase (**SPT**) in Cer de novo synthesis (Han et al., 2009). Gene *SPTSSB* was expressed at lower levels at 9 d relative to -8 d (Figure 2), corresponding to the patterns of most Cer subspecies over time, while the expression of *SPTSSA* increased after parturition, corresponding to the pattern of Cer (23:0) over time. The different expression patterns of the two SPT small subunits over time may suggest that these small subunits could have influenced the fatty acyl-CoA selectivity of SPT, as suggested by Han et al. (2009). Alternatively, the declines in most hepatic Cers over time may have resulted from the increased lipoprotein export of Cer when higher amount NEFA entered liver (Watt et al., 2012), as suggested by the negative correlation between plasma NEFA concentration and hepatic Cer concentrations postpartum. The increased hepatic export of Cer may occur to compensate plasma Cer level, as suggested by Rico et al. (2017), showing the elevation in plasma total Cer and Cer (24:0) concentrations after parturition. The exported Cer may contribute to the regulation of peripheral insulin sensitivity (Rico et al., 2015, 2017). The apparently contradictory negative correlation between hepatic Cer (24:0) and glucose area under curve in IVGTT after parturition may accentuate the role of hepatic lipoprotein export in the regulation of systemic insulin sensitivity.

CONCLUSIONS

The effects of prepartal high-energy intake on the hepatic adaptation of dairy cows were reflected in gene expression and sphingolipid profiles prepartum, while postpartal hepatic gene expression and sphingolipid profiles were not affected. In the absence of change in body condition score, the observed prepartal effects were most likely due to the greater energy balance and decreased hepatic NEFA influx. Specifically, prepartal high-energy feeding increased hepatic lipogenesis before parturition by upregulating *LXR/RXR* pathway and lipogenic gene *THRSP* at gene expression level. Moreover, prepartal high-energy feeding suppressed hepatic inflammatory and acute phase responses before parturition, as supported by the downregulated expression of pro-inflammatory genes *IL1* and *NFKB1* and acute phase protein-coding genes *SAA3*, *HP*, and *LBP*. Subsequently, reduced inflammation in the liver may have contributed to the increased hepatic concentrations of C18-, C20-, C21-, C23-sphingomyelin, and total saturated sphingomyelin through the downregulation of sphingomyelin hydrolysis. Regardless of the diet, the cows displayed an increase in hepatic lipogenesis at gene expression level from 8 d prepartum to 9 d postpartum and decreases in the concentration of most ceramide and sphingomyelin subspecies detected in lipidomic analysis. Collectively, prepartal high-energy feeding did not disturb the hepatic adaptation of dairy cows during the periparturient period.

ACKNOWLEDGMENTS

This study was funded by the Ministry of Agriculture and Forestry (Helsinki, Finland), Suomen Naudanjalostussäätiö Foundation (Hamina, Finland) and by the Future Fund (University of Helsinki). NQ was supported by the AGFOREE doctoral program of the University of Helsinki. The authors are grateful to Juha Suomi and his staff at the research farm of the University of Helsinki for their help in caring for the cows used in this study.

521

REFERENCES

Aiello, R., T. Kenna, and J. Herbein. 1984. Hepatic gluconeogenic and ketogenic interrelationships in the lactating cow. J. Dairy Sci. 67:1707–1715.

Akbar, H., E. Schmitt, M. A. Ballou, M. N. Correa, E. J. Depeters, and J. J. Loor. 2013. Dietary lipid during late-pregnancy and early-lactation to manipulate metabolic and inflammatory gene network expression in dairy cattle liver with a focus on PPARs. Gene Regul. Syst. Biol. 7:103–23.

Bell, A. W., and D. E. Bauman. 1997. Adaptations of glucose metabolism during pregnancy and lactation. J. Mammary Gland Biol. 2:265–278.

Bell, A. 1995. Regulation of organic nutrient metabolism during transition from late pregnancy to early lactation. J. Anim. Sci. 73:2804–2819.

Benjamini, Y., and Y. Hochberg. 2000. On the adaptive control of the false discovery fate in multiple testing with independent statistics. J. Educ. Behav. Stat. 25:60–83.

Bode, J. G., U. Albrecht, D. Haeussinger, P. C. Heinrich, and F. Schaper. 2012. Hepatic acute phase proteins - regulation by IL-6-and IL-1-type cytokines involving STAT3 and its crosstalk with NF-kappa B-dependent signaling. Eur. J. Cell Biol. 91:496–505.

Bionaz, M., E. Trevisi, L. Calamari, F. Librandi, A. Ferrari, and G. Bertoni. 2007. Plasma paraoxonase, health, inflammatory conditions, and liver function in transition dairy cows. J. Dairy Sci. 90:1740–1750.

Chavez, J. A. and S. A. Summers. 2012. A ceramide-centric view of insulin resistance. Cell Metab. 15:585–594.

543 Cui, Y., Z. Liu, X. Sun, X. Hou, B. Qu, F. Zhao, X. Gao, Z. Sun, and Q. Li. 2015. Thyroid hormone
544 responsive protein spot 14 enhances lipogenesis in bovine mammary epithelial cells. In Vitro
545 Cell. Dev. Biol.Anim. 51:586–594.

546 Dann, H. M., N. B. Litherland, J. P. Underwood, M. Bionaz, A. D'Angelo, J. W. McFadden, and J.
547 K. Drackley. 2006. Diets during far-off and close-up dry periods affect periparturient
548 metabolism and lactation in multiparous cows. J. Dairy Sci. 89:3563–3577.

549 De Koster, J., M. Hostens, M. Van Eetvelde, K. Hermans, S. Moerman, H. Bogaert, E. Depreester,
550 W. Van den Broeck and G. Opsomer. 2015. Insulin response of the glucose and fatty acid
551 metabolism in dry dairy cows across a range of body condition scores. J. Dairy Sci. 98:4580–
552 4592.

553 Douglas, G. N., T. R. Overton, H. G. Bateman, H. M. Dann, and J. K. Drackley. 2006. Prepartal
554 plane of nutrition, regardless of dietary energy source, affects periparturient metabolism and
555 dry matter intake in holstein cows. J. Dairy Sci. 89:2141–2157.

556 Drackley, J. K., T. R. Overton, and G. N. Douglas. 2001. Adaptations of glucose and long-chain
557 fatty acid metabolism in liver of dairy cows during the periparturient period. J. Dairy Sci.
558 84:E100–E112.

559 Drackley, J., H. Dann, G. Douglas, N. Guretzky, N. Litherland, J. Underwood, and J. Loor. 2005.
560 Physiological and pathological adaptations in dairy cows that may increase susceptibility to
561 periparturient diseases and disorders. Ital. J. Anim. Sci. 4:323–344.

562 Gross, J. J., F. J. Schwarz, K. Eder, H. A. van Dorland, and R. M. Bruckmaier. 2013. Liver fat
563 content and lipid metabolism in dairy cows during early lactation and during a mid-lactation
564 feed restriction. J. Dairy Sci. 96:5008–5017.

565 Grummer, R. R., D. G. Mashek and A. Hayirli. 2004. Dry matter intake and energy balance in the
566 transition period. Veterinary Clinics of North America: Food Animal Practice. 20:447-470.

567 Han, G., S. D. Gupta, K. Gable, S. Niranjanakumari, P. Moitra, F. Eichler, R. H. Brown Jr., J. M.
568 Harmon, and T. M. Dunn. 2009. Identification of small subunits of mammalian serine
569 palmitoyltransferase that confer distinct acyl-CoA substrate specificities (vol 106, pg 8186,
570 2009). Proc. Natl. Acad. Sci. U. S. A. 106:9931–9931.

571 Herdt, T. 2000. Ruminant adaptation to negative energy balance - influences on the etiology of
572 ketosis and fatty liver. Vet. Clin. North Am. Food Anim. Pract. 16:215–230.

573 Imhasly, S., C. Bieli, H. Naegeli, L. Nystroem, M. Ruetten, and C. Gerspach. 2015. Blood plasma
574 lipidome profile of dairy cows during the transition period. BMC Vet. Res. 11:252.

575 Ingvartsen, K. L. 2006. Feeding- and management-related diseases in the transition cow -
576 physiological adaptations around calving and strategies to reduce feeding-related diseases.
577 Anim. Feed Sci. Technol. 126:175–213.

578 Irizarry, R., B. Hobbs, F. Collin, Y. Beazer-Barclay, K. Antonellis, U. Scherf, and T. Speed. 2003.
579 Exploration, normalization, and summaries of high density oligonucleotide array probe level
580 data. Biostatistics 4:249–264.

581 Jain, N., J. Thatte, T. Braciale, K. Ley, M. O'Connell, and J. K. Lee. 2003. Local-pooled-error test
582 for identifying differentially expressed genes with a small number of replicated microarrays.
583 Bioinformatics 19:1945–1951.

584 Janovick, N. A., Y. R. Boisclair and J. K. Drackley. 2011. Prepartum dietary energy intake affects
585 metabolism and health during the periparturient period in primiparous and multiparous holstein
586 cows 1. J. Dairy Sci. 94:1385–1400.

587 Jenkins, R. W., D. Canals, J. Idkowiak-Baldys, F. Simbari, P. Roddy, D. M. Perry, K. Kitatani, C.
588 Luberto, and Y. A. Hannun. 2010. Regulated secretion of acid sphingomyelinase. Implications
589 for selectivity of ceramide formation. J. Biol. Chem. 285:35706–35718.

590 Ji, P., J. K. Drackley, M. J. Khan and J. J. Loor. 2014. Inflammation- and lipid metabolism-related
591 gene network expression in visceral and subcutaneous adipose depots of Holstein cows. J.
592 Dairy Sci. 97:3441–3448.

593 Jiménez-Marín, Á, M. Collado-Romero, M. Ramirez-Boo, C. Arce, and J. J. Garrido. 2009.
594 Biological pathway analysis by ArrayUnlock and ingenuity pathway analysis. BMC Proc.
595 2009 3 (suppl 4):S6.

596 Jin, J., X. Zhang, Z. Lu, D. M. Perry, Y. Li, S. B. Russo, L. A. Cowart, Y. A. Hannun, and Y.
597 Huang. 2013. Acid sphingomyelinase plays a key role in palmitic acid-amplified inflammatory
598 signaling triggered by lipopolysaccharide at low concentrations in macrophages. Am. J.
599 Physiol. Endocrinol. Metab. 305:E853–E867.

600 Kallio, M. A., J. T. Tuimala, T. Hupponen, P. Klemela, M. Gentile, I. Scheinin, M. Koski, J. Kaki,
601 and E. I. Korpelainen. 2011. Chipster: User-friendly analysis software for microarray and other
602 high-throughput data. BMC Genomics 12:507.

603 Khan, M. J., C. B. Jacometo, D. E. Graugnard, M. N. Correa, E. Schmitt, F. Cardoso, and J. J. Loor.
604 2014. Overfeeding dairy cattle during late-pregnancy alters hepatic PPARalpha-regulated
605 pathways including hepatokines: Impact on metabolism and peripheral insulin sensitivity. Gene
606 Regul. Syst. Biol. 8:97–111.

607 Larsen, P. J., and N. Tennagels. 2014. On ceramides, other sphingolipids and impaired glucose
608 homeostasis. Mol. Metab. 3:252–60.

609 Loor, J. J., H. M. Dann, R. E. Everts, R. Oliveira, C. A. Green, N. A. J. Guretzky, S. L. Rodriguez-
610 Zas, H. A. Lewin, and J. K. Drackley. 2005. Temporal gene expression profiling of liver from
611 periparturient dairy cows reveals complex adaptive mechanisms in hepatic function. Physiol.
612 Genomics 23:217–226.

613 Loor, J. J., H. M. Dann, N. A. J. Guretzky, R. E. Everts, R. Oliveira, C. A. Green, N. B. Litherland,
614 S. L. Rodriguez-Zas, H. A. Lewin, and J. K. Drackley. 2006. Plane of nutrition prepartum
615 alters hepatic gene expression and function in dairy cows as assessed by longitudinal transcript
616 and metabolic profiling. Physiol. Genomics 27:29–41.

617 Lu, Z., Y. Li, J. Jin, X. Zhang, Y. A. Hannun, and Y. Huang. 2015. GPR40/FFA1 and neutral
618 sphingomyelinase are involved in palmitate-boosted inflammatory response of microvascular
619 endothelial cells to LPS. Atherosclerosis 240:163–173.

620 Luke. 2018. Finnish feed tables and feeding recommendations. Accessed Jan. 27, 2018.
621 https://portal.mtt.fi/portal/page/portal/Rehutaulukot/feed_tables_english.

622 Maceyka, M., and S. Spiegel. 2014. Sphingolipid metabolites in inflammatory disease. Nature
623 510:58–67.

624 Mann, S., D. V. Nydam, A. Abuelo, F. A. Leal Yepes, T. R. Overton, and J. J. Wakshlag. 2016.
625 Insulin signaling, inflammation, and lipolysis in subcutaneous adipose tissue of transition dairy
626 cows either overfed energy during the prepartum period or fed a controlled-energy diet. J.
627 Dairy Sci. 99:6737–6752.

628 McArdle, M. A., O. M. Finucane, R. M. Connaughton, A. M. McMorrow, and H. M. Roche. 2013.
629 Mechanisms of obesity-induced inflammation and insulin resistance: Insights into the
630 emerging role of nutritional strategies. Front. Endocrinol. 4:52–52.

631 McCarthy, S. D., S. M. Waters, D. A. Kenny, M. G. Diskin, R. Fitzpatrick, J. Patton, D. C. Wathes,
632 and D. G. Morris. 2010. Negative energy balance and hepatic gene expression patterns in high-
633 yielding dairy cows during the early postpartum period: A global approach. Physiol. Genomics
634 42A:188–199.

635 Merrill, A. H. Jr. 2011. Sphingolipid and glycosphingolipid metabolic pathways in the era of
636 sphingolipidomics. Chem. Rev. 111:6387–6422.

637 Nakagawa, H., O. Yamamoto, S. Oikawa, H. Higuchi, A. Watanabe, and N. Katoh. 1997. Detection
638 of serum haptoglobin by enzyme-linked immunosorbent assay in cows with fatty liver. Res.
639 Vet. Sci. 62:137–141.

640 Nygren, H., T. Seppanen-Laakso, S. Castillo, T. Hyotylainen, and M. Oresic. 2011. Liquid
641 chromatography-mass spectrometry (LC-MS)-based lipidomics for studies of body fluids and
642 tissues. Methods Mol Biol. 708:247–57.

643 Qin, N., T. Kokkonen, S. Salin, T. Seppanen-Laakso, J. Taponen, A. Vanhatalo, and K. Elo. 2017.
644 Prepartal overfeeding alters the lipidomic profiles in the liver and the adipose tissue of
645 transition dairy cows. Metabolomics 13:21.

646 Rico, J. E., V. V. R. Bandaru, J. M. Dorskind, N. J. Haughey, and J. W. McFadden. 2015. Plasma
647 ceramides are elevated in overweight holstein dairy cows experiencing greater lipolysis and
648 insulin resistance during the transition from late pregnancy to early lactation. J. Dairy Sci.
649 98:7757–7770.

650 Rico, J. E., S. S. Samii, A. T. Mathews, J. Lovett, N. J. Haughey and J. W. McFadden. 2017.
651 Temporal changes in sphingolipids and systemic insulin sensitivity during the transition from
652 gestation to lactation. Plos One 12:e0176787.

653 Roche, J. R., S. Meier, A. Heiser, M. D. Mitchell, C. G. Walker, M. A. Crookenden, M. V. Riboni,
654 J. J. Loor and J. K. Kay. 2015. Effects of precalving body condition score and prepartum
655 feeding level on production, reproduction, and health parameters in pasture-based transition
656 dairy cows. J. Dairy Sci. 98:7164-7182.

657 Salin, S., A. Vanhatalo, K. Elo, J. Taponen, R. C. Boston, and T. Kokkonen. 2017. Effects of
658 dietary energy allowance and decline in dry matter intake during the dry period on responses to
659 glucose and insulin in transition dairy cows. J. Dairy Sci. 100: 5266–5280.

660 Saremi, B., A. Al-Dawood, S. Winand, U. Mueller, J. Pappritz, D. von Soosten, J. Rehage, S.
661 Daenicke, S. Haeussler, M. Mielenz, and H. Sauerwein. 2012. Bovine haptoglobin as an
662 adipokine: Serum concentrations and tissue expression in dairy cows receiving a conjugated
663 linoleic acids supplement throughout lactation. Vet. Immunol. Immunopathol. 146:201–211.

664 Saremi, B., M. Mielenz, M. M. Rahman, A. Hosseini, C. Kopp, S. Daenicke, F. Ceciliani, and H.
665 Sauerwein. 2013. Hepatic and extrahepatic expression of serum amyloid A3 during lactation in
666 dairy cows. J. Dairy Sci. 96:6944–6954.

667 Schultz, J., H. Tu, A. Luk, J. Repa, J. Medina, L. Li, S. Schwendner, S. Wang, M. Thoolen, D.
668 Mangelsdorf, K. Lustig, and B. Shan. 2000. Role of LXRs in control of lipogenesis. Genes
669 Dev. 14:2831–2838.

670 Selim, S., T. Kokkonen, J. Taponen, A. Vanhatalo, and K. Elo. 2015. Effect of prepartal ad libitum
671 feeding of grass silage on transcriptional adaptations of the liver and subcutaneous adipose
672 tissue in dairy cows during the periparturient period. J. Dairy Sci. 98:5515–5528.

673 Selim, S., S. Salin, J. Taponen, A. Vanhatalo, T. Kokkonen, and K. T. Elo. 2014. Prepartal dietary
674 energy alters transcriptional adaptations of the liver and subcutaneous adipose tissue of dairy
675 cows during the transition period. Physiol. Genomics 46:328–337.

676 Shahzad, K., M. Bionaz, E. Trevisi, G. Bertoni, S. L. Rodriguez-Zas and J. J. Loor. 2014.
677 Integrative analyses of hepatic differentially expressed genes and blood biomarkers during the
678 peripartal period between dairy cows overfed or restricted-fed energy prepartum. Plos One
679 9:e99757.

680 Shi, H., M. V. Kokoeva, K. Inouye, I. Tzameli, H. Yin, and J. S. Flier. 2006. TLR4 links innate
681 immunity and fatty acid-induced insulin resistance. J. Clin. Invest. 116:3015–3025.

682 Shirasuna, K., H. Takano, K. Seno, A. Ohtsu, T. Karasawa, M. Takahashi, A. Ohkuchi, H. Suzuki,
683 S. Matsubara, H. Iwata, and T. Kuwayama. 2016. Palmitic acid induces interleukin-1 beta

684 secretion via NLRP3 inflammasomes and inflammatory responses through ROS production in
685 human placental cells. J. Reprod. Immunol. 116:104–112.

686 Trevisi, E., M. Amadori, S. Cogrossi, E. Razzuoli, and G. Bertoni. 2012. Metabolic stress and
687 inflammatory response in high-yielding, periparturient dairy cows. Res. Vet. Sci. 93:695–704.

688 Vernon, R. G. 2005. Lipid metabolism during lactation: A review of adipose tissue-liver
689 interactions and the development of fatty liver. J. Dairy Res. 72:460–469.

690 Watt, M. J., A. C. Barnett, C. R. Bruce, S. Schenk, J. F. Horowitz, and A. J. Hoy. 2012. Regulation
691 of plasma ceramide levels with fatty acid oversupply: Evidence that the liver detects and
692 secretes de novo synthesised ceramide. Diabetologia 55:2741–2746.

693 Wong, M., B. Xie, N. Beatini, P. Phu, S. Marathe, A. Johns, P. Golds, E. Hirsch, K. Williams, J.
694 Licinio, and I. Tabas. 2000. Acute systemic inflammation up-regulates secretory
695 sphingomyelinase in vivo: A possible link between inflammatory cytokines and atherogenesis.
696 Proc. Natl. Acad. Sci. USA. 97:8681–8686.

697 Wu, J., C. Wang, S. Li, S. Li, W. Wang, J. Li, Y. Chi, H. Yang, X. Kong, Y. Zhou, C. Dong, F.
698 Wang, G. Xu, J. Yang, J. Gustafsson, and Y. Guan. 2013. Thyroid hormone-responsive SPOT
699 14 homolog promotes hepatic lipogenesis, and its expression is regulated by liver X receptor
700 through a sterol regulatory element-binding protein 1c-dependent mechanism in mice.
701 Hepatology 58:617–628.

702 Xia, J., I. V. Sinelnikov, B. Han, and D. S. Wishart. 2015. MetaboAnalyst 3.0-making
703 metabolomics more meaningful. Nucleic Acids Res. 43:W251–W257.

704 Yao, D. W., J. Luo, Q. Y. He, M. Wu, H. B. Shi, H. Wang, M. Wang, H. F. Xu, and J. J. Loor.
705 2016. Thyroid hormone responsive (THRSP) promotes the synthesis of medium-chain fatty
706 acids in goat mammary epithelial cells. J. Dairy Sci. 99:3124–3133.

707

Table 1. Concentration of sphingolipid subclasses that showed significant difference ($P < 0.05$) or tendencies towards significant ($P < 0.10$) difference between the feeding groups at 8 d prior to parturition (-8 d) and 9 d postpartum (9 d).

		Mean[2]			*P*-value		
Lipid subclass		CON	HIGH	SEM	Diet	Day	Diet × Day
Cer (23:0)[1]	-8 d	-2.02	-1.84	0.057	0.088	0.030	0.429
	9 d	-1.68	-1.66				
Cer (23:1)	-8 d	-3.97	-3.77	0.075	0.099	0.014	0.415
	9 d	-4.27	-4.24				
Cer (24:1)	-8 d	-3.60	-3.22 *	0.090	0.080	0.540	0.083
	9 d	-3.54	-3.41				
Cer (25:1)	-8 d	-5.31	-4.91 *	0.081	0.052	0.025	0.231
	9 d	-5.46	-5.34				
Saturated Cer	-8 d	-2.53	-2.22	0.076	0.081	0.066	0.161
	9 d	-2.63	-2.54				
SM (C18)	-8 d	-4.44	-4.23 †	0.062	0.007	0.011	0.542
	9 d	-4.60	-4.49				
SM (C20)	-8 d	-5.93	-5.62 *	0.093	0.004	0.281	0.541
	9 d	-5.70	-5.56				
SM (C21)	-8 d	-5.40	-4.97 †	0.106	0.035	0.506	0.624
	9 d	-5.21	-4.96				
SM (C23)	-8 d	-2.40	-1.93 *	0.078	<0.001	0.614	0.193
	9 d	-2.33	-2.13				
Saturated SM	-8 d	-0.86	-0.51 *	0.080	0.004	0.167	0.430
	9 d	-0.97	-0.78				

Label and abbreviations: HIGH, high-energy feeding group (targeted to 150% of the energy requirement of pregnant dairy); CON, controlled-energy feeding group (100% of the energy requirement of pregnant dairy cow); †,* ,** Statistical significance of the treatment effect is indicated in each row, † = P < 0.10; * = P < 0.05; ** = P < 0.01; SEM, standard error of the mean; Cer, ceramide; SM, sphingomyelin. 1. The content in the bracket indicates the fatty acid composition. 2. The mean values in the table were log2-transformed from the original concentrations (μmol/g tissue).

716 Table 2. Summary of the most significant differentially expressed genes (DEGs), diseases, and
717 biological functions in Ingenuity Pathway Analyses (IPAs).

Analyses	-8 d		1 d		9 d	
Top 5 upregulated molecules						
	Molecule	Log2-fold	Molecule	Log2-fold	Molecule	Log2-fold
	BOLA-DQB1	1.938	*GNMT*	1.736	*BOLA-DQA2*	1.447
	BOLA-DQB2	1.484	*BOLA-DQB1*	1.551	*BOLA-DQB1*	1.343
	MBOAT2	1.124	*CRIP3*	1.328	*PRSS2*	1.232
	SLC11A1	1.108	*EGR1*	1.278	*CYP11A1*	0.922
	SOCS3	1.040	*CYP11A1*	1.168	*HP*	0.843
Top 5 downregulated molecules						
	Molecule	Log2-fold	Molecule	Log2-fold	Molecule	Log2-fold
	S100A10	-1.878	*BOLA-B*	-2.283	*PCK1*	-1.996
	UGT3A1	-1.758	*CPT1A*	-2.059	*BOLA-B*	-1.597
	CPT1A	-1.519	*S100A10*	-1.889	*ASPA*	-1.503
	SNCA	-1.428	*BOLA-DQA2*	-1.889	*CPQ*	-1.465
	BOLA-B	-1.416	*SNCA*	-1.620	*S100A10*	-1.417
Top 5 Disease and biological functions						
	Lipid metabolism		Lipid metabolism		Energy production	
	Small-molecule biochemistry		Molecular transport		Inflammatory disease	
	Vitamin and mineral metabolism		Small-molecule biochemistry		Immunological disease	
	Connective-tissue disorders		Cellular function and maintenance		Cell-to-cell signaling and interaction	
	Inflammatory diseases		Cardiovascular disease		Connective-tissue disorders	

718

719 *BOLA-DQB1*, *histocompatibility* complex, class II, *DQ beta*, *type 1*. *BOLA-DQB2*,
720 *histocompatibility complex, class II, DQ beta, type 2*. *MBOAT2*, *membrane-bound O-*

721 *acyltransferase domain containing type 2*. *SLC11A1, solute carrier family 11 member A1*. SOCS3,
722 *suppressor of cytokine signaling 3*. *S100A10, S100 calcium-binding protein A10*. *UGT3A1, UDP*
723 *glycosyltransferase family 3, polypeptide A1*. *CPT1A, carnitine palmitoyltransferase 1A*. SNCA,
724 *synuclein alpha*. *BOLA-B, major histocompatibility complex, class I, B*. GNMT, *glycine N-*
725 *methyltransferase*. *CRIP3, cysteine-rich protein 3*. *EGR1, early growth response 1*. *CYP11A1,*
726 *cytochrome P450, family 11, subfamily A, polypeptide 1*. *BOLA-DQA2, histocompatibility complex,*
727 *class II, DQ alpha 2*. *PRSS2, protease, serine S2*. *HP, haptoglobin*. *PCK1, phosphoenolpyruvate*
728 *carboxykinase 1*. *ASPA, aspartoacylase*. *CPQ, carboxypeptidase Q*.

729

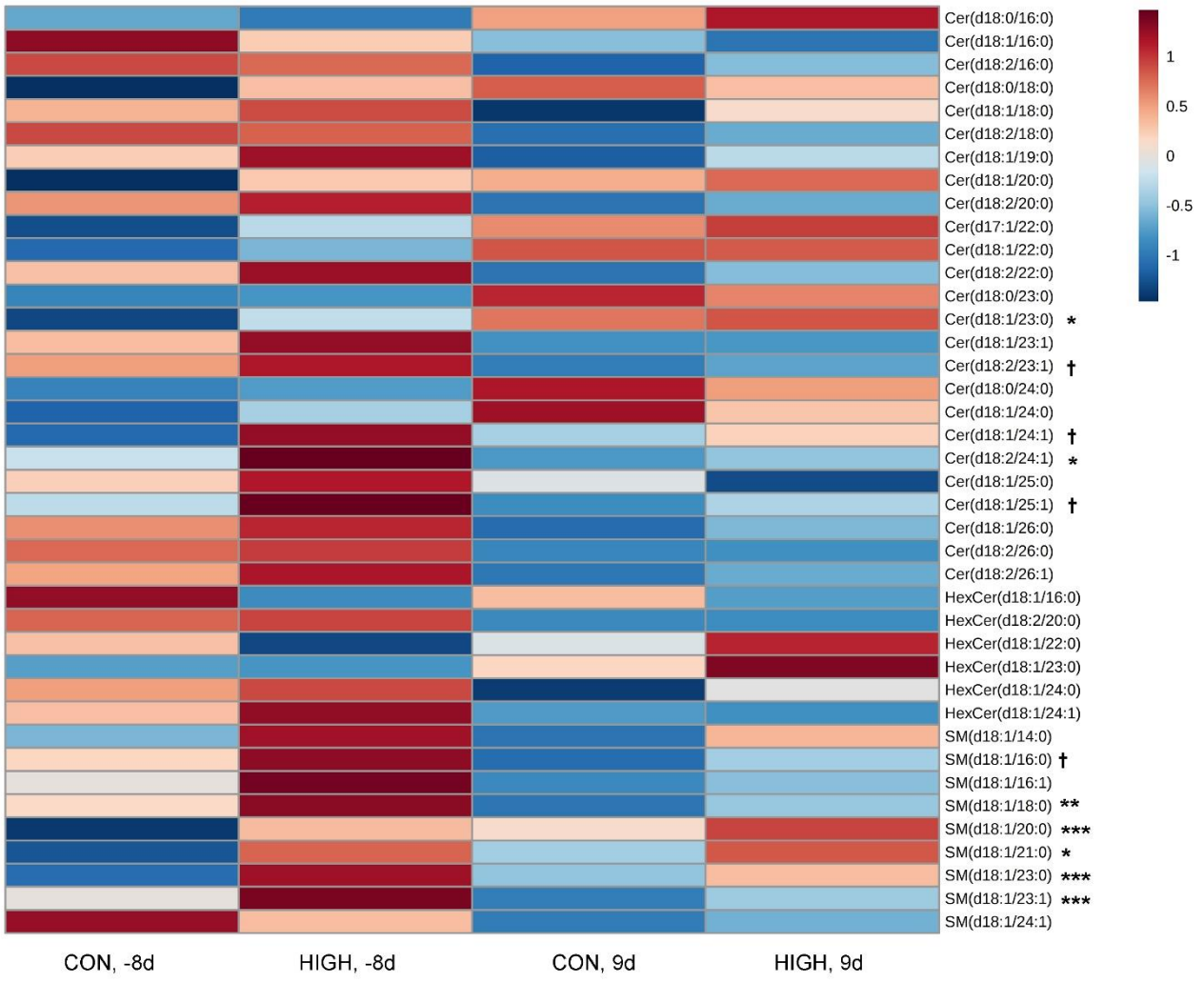

730

731

732 Figure 1. Heatmap of sphingolipid concentrations in the controlled-energy (CON) feeding group and
733 high-energy (HIGH) feeding group at 8 d prior to the predicted parturition (-8 d) and 9 d after the
734 actual parturition (9 d). The concentration of sphingolipids was scaled based on their magnitude,
735 represented by the intensity of grey color. Comparisons should be made within sphingolipid
736 subspecies. The names of subspecies were formatted as sphingolipid type (sphingosine
737 composition/fatty acid composition). Cer, ceramide. HexCer, hexosylceramide. SM, sphingomyelin.
738 †,* ,** Statistical significance of the treatment effect is indicated in each row, † = $P < 0.10$; * = $P <$
739 0.05; ** = $P < 0.01$, *** = $P < 0.005$;

740

741

742

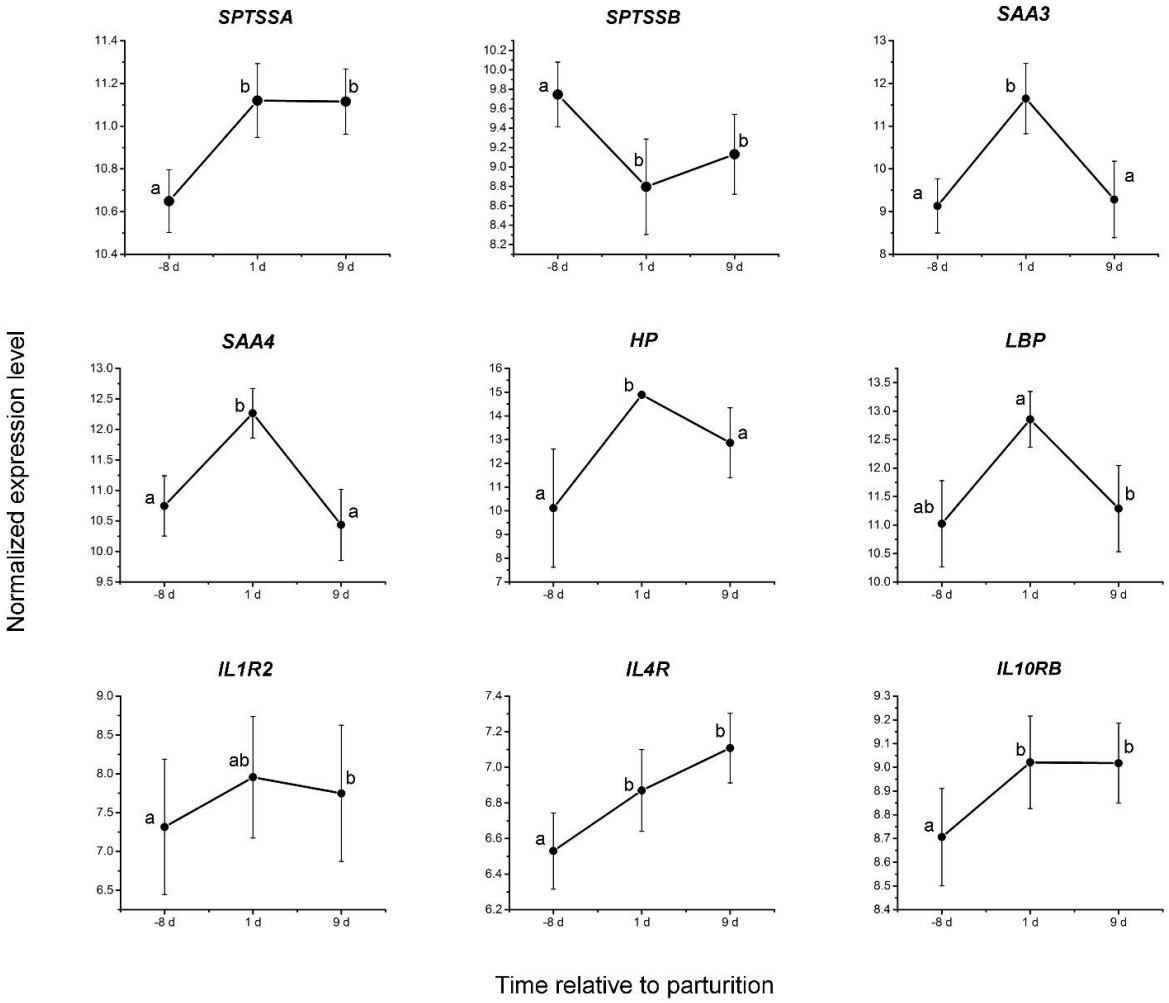

743

744

745 Figure 2. Normalized expression level of genes involved in ceramide metabolism, acute phase
746 response, and inflammatory response at 8 d prior to the predicted parturition (-8 d), 1 d after the actual
747 parturition (1 d), and 9 d after the actual parturition (9 d). The different letters indicate significant
748 differences ($P < 0.05$). *SPTSSA*, *serine palmitoyltransferase small subunit A*. *SPTSSB*, *serine*
749 *palmitoyltransferase small subunit B*. *SAA3*, *serum amyloid A3*. *SAA4*, *serum amyloid A4*. *HP*,
750 *haptoglobin*. *LBP*, *lipopolysaccharide-binding protein*. *IL1R2*, *interleukin 1 receptor type 2*. *IL4R*,
751 *interleukin 4 receptor*. *IL10RB*, *interleukin 10 receptor subunit beta*.

752

753

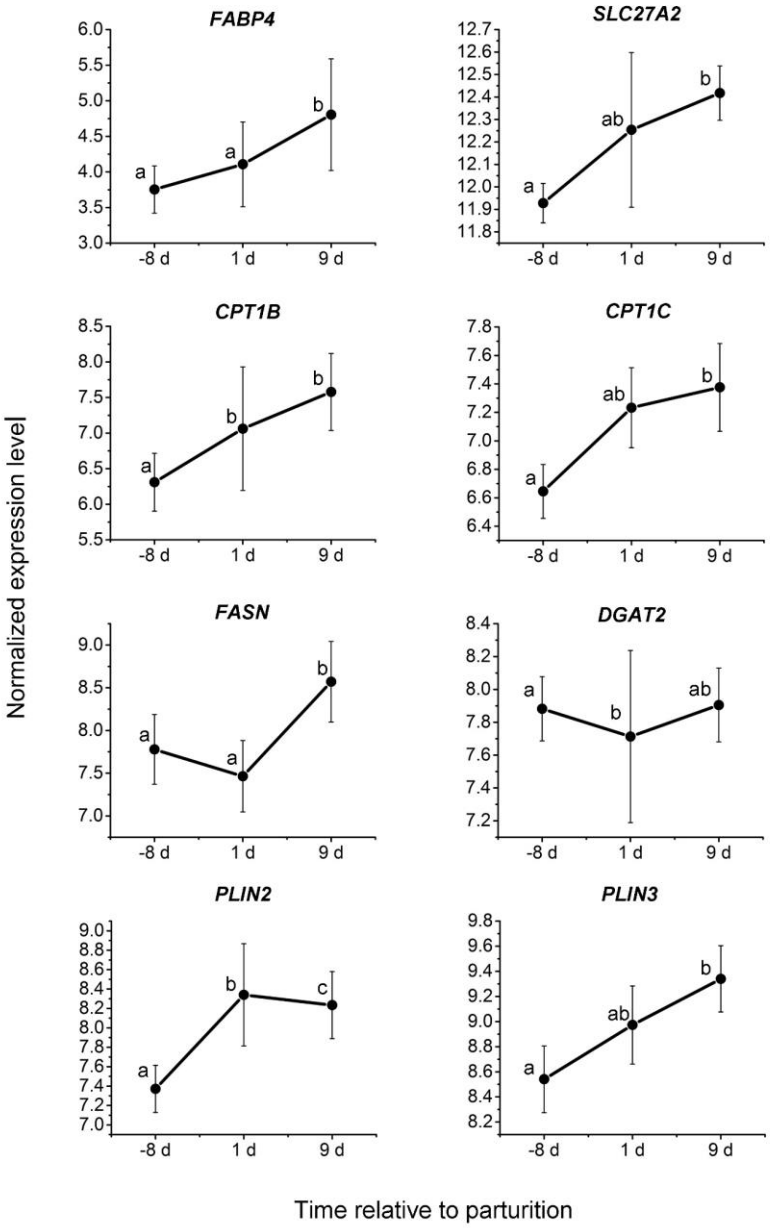

754

755

756 Figure 3. Normalized expression level of genes involved in lipid metabolism at 8 d prior to the
757 predicted parturition (-8 d), 1 d after the actual parturition (1 d), and 9 d after the actual parturition (9
758 d). The Different letters indicate significant differences ($P < 0.05$). *FABP4, fatty acid binding protein*
759 *4*. *SLC27A2, solute carrier family 27 member A2*. *CPT1B, carnitine palmitoyltransferase 1B*. *CPT1C,*
760 *carnitine palmitoyltransferase 1C*. *DGAT2, diacylglycerol O-acyltransferase 2*. *FASN, fatty acid*
761 *synthase*. *PLIN2, perilipin 2*. *PLIN3, perilipin 3*.

Supplemental Table S1.
Repeated-measures ANOVA of sphingolipid subclasses in the liver.

	Mean[3]			*P*-value		
Lipid subclass	CON	HIGH	SEM	Diet	Day	Diet×Day
Cer (16:0)[1]						
-8 d	-3.21	-3.35	0.104	0.521	0.128	0.766
9 d	-3.49	-3.55				
Cer (18:0)						
-8 d	-4.46	-4.36	0.122	0.218	0.042	0.573
9 d	-4.92	-4.64				
Cer (19:0)						
-8 d	-7.44	-7.36	0.058	0.275	0.188	0.903
9 d	-7.56	-7.50				
Cer (20:0)						
-8 d	-5.70	-5.43	0.108	0.288	0.283	0.510
9 d	-5.39	-5.36				
Cer (22:0)						
-8 d	-2.22	-2.09	0.069	0.134	0.134	0.639
9 d	-1.98	-1.96				
Cer (23:0)						
-8 d	-2.02	-1.84	0.057	0.088	0.030	0.429
9 d	-1.68	-1.66				
Cer (23:1)						
-8 d	-3.97	-3.77	0.075	0.099	0.014	0.415
9 d	-4.26	-4.24				
Cer (24:0)						
-8 d	-1.81	-1.71	0.085	0.972	0.313	0.529
9 d	-1.56	-1.65				
Cer (24:1)						
-8 d	-3.60	-3.22	* 0.090	0.080	0.540	0.083
9 d	-3.54	-3.41				
Cer (25:0)						
-8 d	-3.81	-3.63	0.096	0.488	0.088	0.159
9 d	-3.87	-4.20				
Cer (25:1)						
-8 d	-5.31	-4.91	* 0.081	0.052	0.025	0.231
9 d	-5.46	-5.34				
Cer (26:0)						
-8 d	-3.27	-3.03	0.159	0.226	<0.001	0.865
9 d	-4.58	-4.25				
Cer (26:1)						
-8 d	-10.62	-10.31	0.126	0.191	<0.001	0.823
9 d	-11.63	-11.40				
Saturated Cer						
-8 d	0.15	0.26	0.066	0.361	0.849	0.585
9 d	0.24	0.22				
MUFA-Cer						
-8 d	-2.53	-2.22	* 0.076	0.081	0.066	0.161
9 d	-2.63	-2.54				
Cer (d17:1)[2]						
-8 d	-4.56	-4.34	0.067	0.327	0.044	0.572
9 d	-4.17	-4.11				
Cer (d18:0)						

-8 d	-5.38	-5.36		0.145	0.699	0.014	0.668
9 d	-4.63	-4.80					
Cer (d18:1)							
-8 d	0.21	0.35		0.062	0.223	0.906	0.496
9 d	0.27	0.26					
Cer (d18:2)							
-8 d	-4.08	-3.83		0.082	0.101	<0.001	0.659
9 d	-4.70	-4.56					
SM (C14)							
-8 d	-6.26	-5.88	†	0.111	0.111	0.547	0.674
9 d	-6.28	-6.01					
SM (C16)							
-8 d	-1.75	-1.48		0.098	0.081	0.037	0.759
9 d	-2.06	-1.87					
SM (C18)							
-8 d	-4.44	-4.23	†	0.062	0.007	0.011	0.542
9 d	-4.60	-4.49					
SM (C20)							
-8 d	-5.93	-5.62	*	0.093	0.004	0.281	0.541
9 d	-5.70	-5.56					
SM (C21)							
-8 d	-5.40	-4.99	†	0.106	0.035	0.506	0.624
9 d	-5.21	-4.96					
SM (C23)							
-8 d	-2.40	-1.93	*	0.078	<0.001	0.614	0.193
9 d	-2.33	-2.13					
SM (C24)							
-8 d	-4.05	-4.21		0.104	0.631	0.036	0.284
9 d	-4.42	-4.35					
Saturated SM							
-8 d	-0.86	-0.51	*	0.080	0.004	0.167	0.430
9 d	-0.97	-0.78					
MUFA-SM							
-8 d	-3.33	-3.27		0.076	0.155	0.002	0.758
9 d	-3.69	-3.58					

1. The content in the bracket indicates the fatty acid composition. 2. The content in the bracket starting with d indicates the sphingosine composition. 3. The mean values in the table were log2-transformed from the original concentrations (μmol/g tissue). 4. Label and abbreviations: †,* ,** Statistical effects of diet in the same row, † = $P < 0.10$; * = $P < 0.05$; ** = $P < 0.01$; CON, controlled-energy feeding group; HIGH, high-energy feeding group; SEM, standard error of the mean; Cer, ceramide; SM, sphingomyelin.

Supplemental Table S2.

Differentially expressed genes (DEGs) mapped in Ingenuity Pathway Analyses (IPAs) at different time points.

Affimetrix code	Gene	Symbol	Expression profile	*P*- value[1]	Log_2 fold[2]
-8 d					
Bt.10056.1.S1_at	Eukaryotic Translation Initiation Factor 2-Alpha Kinase 3	EIF2AK3	Down-regulated	7.00E-05	-0.632
Bt.10340.1.S1_at	G Protein-Coupled Receptor 126	GPR126	Down-regulated	0.024505	-0.442
Bt.1201.1.A1_at	Fetuin B	FETUB	Down-regulated	0.009479	-0.290
Bt.1229.1.S1_at	Apolipoprotein A-I	APOA1	Down-regulated	0	-0.622
Bt.12519.1.S1_at	Flavin Containing Monooxygenase 3	FMO3	Down-regulated	0.007373	-1.400
Bt.12553.1.S1_at	Haptoglobin	HP	Down-regulated	0	-1.036
Bt.12770.1.A1_at	Synuclein, Alpha	SNCA	Down-regulated	0	-1.428
Bt.13367.1.A1_at	X Inactive Specific Transcript	XIST	Down-regulated	0.008764	-0.340
Bt.13622.1.A1_at	N/A	LOC505099	Up-regulated	0.024878	0.606
Bt.13651.2.A1_at	X-Prolyl Aminopeptidase (Aminopeptidase P) 2, Membrane-Bound	XPNPEP2	Up-regulated	0.026712	0.608
Bt.13821.1.S1_at	Adenylate Kinase 4	AK4	Down-regulated	0	-1.226
Bt.14572.1.A1_at	Doublecortin-Like Kinase 1	DCLK1	Down-regulated	0.022095	-0.402
Bt.15748.1.A1_at	Arv1 Homolog	ARV1	Down-regulated	0.001794	-0.562
Bt.15842.1.S1_at	Thyroid Hormone-Inducible Hepatic Protein Spot 14	THRSP	Up-regulated	0.001116	0.874
Bt.15890.1.S1_at	Apolipoprotein A-Iv	APOA4	Up-regulated	0	0.296
Bt.16101.1.S1_at	Granulysin	GNLY	Up-regulated	0.024327	0.136
Bt.16399.1.A1_at	Betaine--Homocysteine S-Methyltransferase	BHMT	Down-regulated	0.006515	-0.628
Bt.16582.1.A1_at	Cytochrome P450, Family 2, Subfamily C, Polypeptide 9	CYP2C9	Up-regulated	0.000151	0.372
Bt.16621.1.A1_at	Interleukin 1, Alpha	IL1A	Down-regulated	8.00E-05	-0.790
Bt.17368.1.A1_at	Purinergic Receptor P2Y, G-Protein Coupled, 14	P2RY14	Down-regulated	3.80E-05	-0.340
Bt.17610.1.A1_at	Chromosome 19 Open Reading Frame 80	C19orf80	Up-regulated	0.005072	0.438
Bt.18083.1.S1_at	3-Hydroxyacyl-Coa Dehydratase 4	PTPLAD2	Down-regulated	7.90E-05	-0.998
Bt.18231.1.S1_at	Cytochrome P450, Family 2, Subfamily C, Polypeptide 9	CYP2C9	Up-regulated	8.00E-06	0.702
Bt.18564.1.A1_at	Alcohol Dehydrogenase 1C (Class I), Gamma Polypeptide	ADH1C	Up-regulated	0.007605	0.598
Bt.19822.1.A1_at	Aldo-Keto Reductase Family 1, Member B10	AKR1B10	Up-regulated	0.015495	0.102
Bt.19825.1.S1_at	Glucuronosyltransferase 2B17	UGT2B17	Down-regulated	3.50E-05	-1.030
Bt.1983.1.S1_at	Egf-Like Module-Containing Mucin-Like Hormone Receptor-Like 1	EMR1	Up-regulated	0.001005	0.732
Bt.20295.1.A1_at	Follistatin	FST	Down-regulated	0.002145	-1.340
Bt.20989.1.S1_at	Nicotinamide Nucleotide Adenylyltransferase 2	NMNAT2	Down-regulated	0	-1.066
Bt.2120.1.S1_at	Carboxypeptidase Q	CPQ	Down-regulated	0.00131	-0.952
Bt.2120.2.S1_at	Carboxypeptidase Q	CPQ	Down-regulated	0.008034	-0.918
Bt.21243.1.A1_at	Inter-Alpha-Trypsin Inhibitor Heavy Chain 3	ITIH3	Down-regulated	0	-0.906
Bt.21997.1.S1_at	Protein Phosphatase, Mg2+/Mn2+ Dependent, 1K	PPM1K	Down-regulated	0.000165	-0.696
Bt.22149.1.S1_at	Family With Sequence Similarity 174, Member B	FAM174B	Down-regulated	4.80E-05	-0.730
Bt.22487.1.S1_at	Alpha-2-Glycoprotein 1, Zinc-Binding	AZGP1	Down-regulated	0.000182	-0.416
Bt.22487.3.S1_at	Alpha-2-Glycoprotein 1, Zinc-Binding	AZGP1	Up-regulated	7.50E-05	1.018
Bt.22763.1.S1_at	3-Hydroxy-3-Methylglutaryl-Coa Synthase 1	HMGCS1	Down-regulated	6.00E-05	-0.624
Bt.23042.1.S1_at	Metallothionein 1A	MT1A	Down-regulated	0	-0.212
Bt.23094.4.S1_at	Aldo-Keto Reductase Family 1, Member C3	AKR1C3	Up-regulated	0.015355	0.722
Bt.23204.1.S1_at	Glutathione S-Transferase Theta 1	GSTT1	Up-regulated	6.80E-05	0.848
Bt.23992.1.A1_at	Adenylate Kinase 4	AK4	Down-regulated	0	-1.092
Bt.24181.1.S1_at	Lipopolysaccharide Binding Protein	LBP	Down-regulated	0.00613	-0.506
Bt.24570.1.S1_at	N-Acylethanolamine Acid Amidase	NAAA	Up-regulated	2.00E-05	0.718
Bt.24600.1.S1_at	Suppressor Of Cytokine Signaling 3	SOCS3	Up-regulated	0.000398	1.040
Bt.25303.1.A1_at	N/A	LOC1003366(	Up-regulated	0.002632	0.702
Bt.2592.1.A1_x_at	Mhc Class I Heavy Chain	BOLA	Up-regulated	0.01779	0.178
Bt.27066.1.A1_at	Insulin Receptor Substrate 1 *	IRS1 *[3]	Down-regulated	0.1	-0.539
Bt.278.1.S1_at	Serum Amyloid A1	SAA1	Down-regulated	0	-0.838
Bt.28011.1.S1_at	Major Histocompatibility Complex, Class Ii, Drb3	BOLA-DRB3	Up-regulated	6.00E-05	1.252
Bt.28208.1.S1_at	Fructose-1,6-Bisphosphatase 2	FBP2	Down-regulated	0	-0.740
Bt.28243.1.S1_a_at	Vanin 1	VNN1	Up-regulated	0.015483	0.634
Bt.28521.1.S1_at	Annexin A13	ANXA13	Down-regulated	4.00E-06	-0.722
Bt.2859.1.A1_at	Set Domain Containing 9	SETD9	Up-regulated	0.010502	0.912
Bt.28878.1.S1_at	Aspartoacylase	ASPA	Down-regulated	0	-1.368
Bt.2896.1.A1_at	Glutathione S-Transferase M1	GSTM1	Up-regulated	1.60E-05	0.540
Bt.29660.1.A1_at	Hydroxysteroid (17-Beta) Dehydrogenase 4	HSD17B4	Up-regulated	0.001335	0.492
Bt.29815.1.A1_at	Mhc Class I Heavy Chain	BOLA	Down-regulated	0.001868	-0.320
Bt.29815.1.S1_x_at	Mhc Class I Heavy Chain	BOLA	Down-regulated	0	-1.416

Bt.3115.1.A1_at	Aspartylglucosaminidase	AGA	Down-regulated	0	-0.434
Bt.3311.1.S1_at	N/A	LOC1019039(	Up-regulated	0.038588	0.486
Bt.350.1.S1_at	Histocompatibility Complex, Class Ii, Dq Beta, Type 1	BOLA-DQB1	Up-regulated	0	0.822
Bt.350.1.S1_x_at	Histocompatibility Complex, Class Ii, Dq Beta, Type 1	BOLA-DQB1	Up-regulated	0	0.510
Bt.3809.1.S1_at	Lactate Dehydrogenase A	LDHA	Down-regulated	0.016101	-0.668
Bt.3862.1.S1_a_at	Peroxisome Proliferator-Activated Receptor Gamma *	PPARG *	Down-regulated	0.09	-1.264
Bt.4137.1.A1_at	G0/G1 Switch 2	G0S2	Up-regulated	0.03592	0.516
Bt.4314.1.S1_at	Annexin A2	ANXA2	Down-regulated	0.000105	-0.534
Bt.4391.1.S2_at	Solute Carrier Family 2 (Facilitated Glucose Transporter), Member 4	GLUT4	Down-regulated	0.1	-1.742
Bt.4594.1.S1_at	Mhc Class Ii Antigen	BLA-DQB	Up-regulated	0	1.938
Bt.4751.1.S1_a_at	Major Histocompatibility Complex, Class Ii, Dq Alpha 2	BOLA-DQA2	Up-regulated	0	1.484
Bt.4751.2.S1_a_at	Major Histocompatibility Complex, Class Ii, Dq Alpha 2	BOLA-DQA2	Up-regulated	0	0.726
Bt.4802.1.S1_at	Lactotransferrin	LTF	Up-regulated	0.000104	1.012
Bt.4852.1.S1_at	Glutathione S-Transferase M1	GSTM1	Up-regulated	0.00039	0.554
Bt.4939.1.S1_at	Secreted Frizzled-Related Protein 2	SFRP2	Down-regulated	0	-0.284
Bt.5037.1.S1_at	S100 Calcium-Binding Protein A10	S100A10	Down-regulated	0	-1.580
Bt.5037.1.S2_at	S100 Calcium-Binding Protein A10	S100A10	Down-regulated	0	-1.878
Bt.5329.1.S1_at	Transmembrane Protein 254	TMEM254	Down-regulated	0.003086	-0.480
Bt.5329.2.S1_at	Transmembrane Protein 254	TMEM254	Down-regulated	0.001794	-0.424
Bt.5362.2.S1_a_at	Serpin Peptidase Inhibitor, Clade A (Alpha-1 Antiproteinase, Antitrypsin), Member 3	SERPINA3-7	Down-regulated	0.004468	-0.170
Bt.5373.1.S1_at	Solute Carrier Family 11 (Proton-Coupled Divalent Metal Ion Transporter), Member 1	SLC11A1	Up-regulated	0.000524	1.108
Bt.628.1.S1_at	Transmembrane Emp24 Protein Transport Domain Containing 6	TMED6	Up-regulated	0.000103	0.510
Bt.647.1.S1_at	Myotrophin	MTPN	Up-regulated	0.003822	0.562
Bt.6636.1.S1_at	Udp Glycosyltransferase 3 Family, Polypeptide A1	UGT3A1	Down-regulated	0.004702	-1.758
Bt.7033.2.S1_a_at	Folate Receptor 1	FOLR1	Down-regulated	0.006555	-0.462
Bt.7033.2.S1_at	Folate Receptor 1	FOLR1	Down-regulated	0.020289	-0.418
Bt.7056.1.S1_at	Hemoglobin Delta	HBB	Up-regulated	0	0.830
Bt.8669.1.S1_at	Membrane Bound O-Acyltransferase Domain Containing 2	MBOAT2	Up-regulated	0	1.124
Bt.8669.2.S1_at	Membrane Bound O-Acyltransferase Domain Containing 2	MBOAT2	Up-regulated	0	1.104
Bt.9289.2.S1_at	Carnitine Palmitoyltransferase 1A *	CPT1A *	Down-regulated	0.04	-1.519
Bt.9309.1.A1_at	Nuclear Factor Kappa B1 *	NFKB1 *	Down-regulated	0.04	-1.177
Bt.9569.1.S1_at	Epithelial Cell Adhesion Molecule	EPCAM	Up-regulated	0.001794	0.202
Bt.9699.1.S1_at	Cytochrome P450, Family 26, Subfamily A, Polypeptide 1	CYP26A1	Down-regulated	0.002145	-0.222
Bt.9807.1.S1_at	Glycoprotein (Transmembrane) Nmb	GPNMB	Up-regulated	0.001335	0.878
1 d					
Bt.12768.1.S1_at	Phosphoenolpyruvate Carboxykinase 1 *	PCK1 *	Down-regulated	0.006	-1.520
Bt.12770.1.A1_at	Synuclein, Alpha	SNCA	Down-regulated	0	-1.620
Bt.13821.1.S1_at	Adenylate Kinase 4	AK4	Up-regulated	0.000171	0.891
Bt.15890.1.S1_at	Apolipoprotein A-Iv	APOA4	Down-regulated	0	-1.216
Bt.17195.1.A1_at	N/A	LOC1001390(	Up-regulated	0.013176	0.270
Bt.17242.1.A1_at	Cytochrome P450, Family 2, Subfamily B, Polypeptide 6	CYP2B6	Down-regulated	0	-1.363
Bt.20432.1.S1_at	Serpin Peptidase Inhibitor, Clade B (Ovalbumin), Member 8	SERPINB8	Down-regulated	0.002371	-0.978
Bt.20919.2.A1_at	Glycine N-Methyltransferase	GNMT	Up-regulated	0	1.736
Bt.20919.3.S1_at	Glycine N-Methyltransferase	GNMT	Up-regulated	4.00E-05	1.398
Bt.20989.1.S1_at	Nicotinamide Nucleotide Adenylyltransferase 2	NMNAT2	Down-regulated	4.40E-05	-0.888
Bt.21113.1.S1_a_at	Carnitine Palmitoyltransferase 1B (Muscle)	CPT1B	Down-regulated	0.001235	-1.141
Bt.2120.1.S1_at	Carboxypeptidase Q	CPQ	Down-regulated	6.00E-06	-1.125
Bt.2120.2.S1_at	Carboxypeptidase Q	CPQ	Down-regulated	2.20E-05	-1.198
Bt.215.1.S1_at	2	BOLA-DQA2	Down-regulated	0	-1.603
Bt.22265.1.S1_at	Early Growth Response 1	EGR1	Up-regulated	0	1.278
Bt.22487.3.S1_at	N/A	LOC1008482(	Down-regulated	0	-1.177
Bt.22629.1.A1_at	Chromosome 21 Open Reading Frame 62	C21orf62	Down-regulated	0.002005	-1.119
Bt.22694.1.A1_at	Apolipoprotein A-V	APOA5	Down-regulated	0.019349	-0.762
Bt.2282.1.S1_a_at	Cysteine-Rich Protein 3	CRIP3	Up-regulated	0.000755	1.328
Bt.22867.2.A1_at	1	BOLA-DQA1	Down-regulated	0.002057	-0.238
Bt.23042.1.S1_at	Metallothionein 1A	MT1A	Up-regulated	0	1.058
Bt.23514.1.S1_at	Alpha-2-Macroglobulin	A2M	Up-regulated	0.005514	0.861
Bt.23992.1.A1_at	Adenylate Kinase 4	AK4	Up-regulated	0.006441	0.881
Bt.24199.1.A1_s_at	Serpin Peptidase Inhibitor, Clade A	UTMP	Up-regulated	0	1.456

Bt.24293.1.A1_at	Betaine--Homocysteine S-Methyltransferase	BHMT	Down-regulated	0.006441	-0.484
Bt.24813.1.A1_at	N/A	LOC532442	Up-regulated	0.005647	0.687
Bt.24827.1.A1_at	N/A	LOC509808	Down-regulated	1.00E-06	-1.506
Bt.25099.1.A1_at	Phosphoserine Phosphatase	PSPH	Up-regulated	4.90E-05	0.983
Bt.25669.1.S1_at	Mucolipin 2	MCOLN2	Up-regulated	0.000903	1.033
Bt.27066.1.A1_at	Insulin Receptor Substrate 1 *	IRS1 *	Up-regulated	0.03	0.103
Bt.27645.1.A1_at	Isthmin 1, Angiogenesis Inhibitor	ISM1	Down-regulated	0.004	-1.488
Bt.28208.1.S1_at	Fructose-1,6-Bisphosphatase 2	FBP2	Down-regulated	0	-0.852
Bt.28278.1.S1_at	Angiotensin I Converting Enzyme 2	ACE2	Down-regulated	0.017581	-1.053
Bt.28521.1.S1_at	Annexin A13	ANXA13	Down-regulated	0.001291	-1.238
Bt.28744.1.S1_at	Guanylate Binding Protein 4	GBP4	Up-regulated	0.014035	0.957
Bt.28965.1.A1_at	Signal Sequence Receptor, Alpha	SSR1	Up-regulated	0.012769	0.880
Bt.29087.1.S1_at	Atp-Binding Cassette, Sub-Family G (White), Member 8	ABCG8	Up-regulated	0.041267	0.870
Bt.29345.1.A1_at	Dead (Asp-Glu-Ala-Asp) Box Polypeptide 10	DDX10	Down-regulated	0.012769	-1.278
Bt.29815.1.S1_x_at	Major Histocompatibility Complex, Class I, B	BOLA-B	Down-regulated	0	-2.283
Bt.350.1.S1_at	Histocompatibility Complex, Class Ii, Dq Beta, Type 1	BOLA-DQB1	Up-regulated	0	1.091
Bt.350.1.S1_x_at	Histocompatibility Complex, Class Ii, Dq Beta, Type 1	BOLA-DQB1	Up-regulated	6.70E-05	1.054
Bt.3551.1.S1_at	Solute Carrier Family 17 (Vesicular Nucleotide Transporter), Member 9	SLC17A9	Up-regulated	0.008889	1.070
Bt.4404.1.A1_at	Protease, Serine, 2 (Trypsin 2)	PRSS2	Up-regulated	0	0.950
Bt.4594.1.S1_at	Histocompatibility Complex, Class Ii, Dq Beta, Type 1	BOLA-DQB1	Up-regulated	0	1.551
Bt.4751.1.S1_a_at	2	BOLA-DQA2	Up-regulated	0	1.399
Bt.5037.1.S1_at	S100 Calcium-Binding Protein A10	S100A10	Down-regulated	0.000124	-1.551
Bt.5037.1.S2_at	S100 Calcium-Binding Protein A10	S100A10	Down-regulated	0	-1.889
Bt.5318.1.S1_at	Retinol Binding Protein 4 *	RBP4 *	Down-regulated	0.03	-0.091
Bt.5970.1.S1_a_at	S100 Calcium Binding Protein A2	S100A2	Up-regulated	0.015226	0.923
Bt.7190.1.S1_at	Cytochrome P450, Family 11, Subfamily A, Polypeptide 1	CYP11A1	Up-regulated	4.90E-05	1.168
Bt.7490.1.A1_at	Methylenetetrahydrofolate Dehydrogenase (Nadp+ Dependent) 1-Like	MTHFD1L	Down-regulated	0	-0.918
Bt.9289.2.S1_at	Carnitine Palmitoyltransferase 1A *	CPT1A *	Down-regulated	0.02	-2.059
Bt.9309.1.A1_at	Nuclear Factor Kappa B1 *	NFKB1 *	Down-regulated	0.03	-1.192

9d

Bt.10371.1.S1_at	Cysteine Sulfinic Acid Decarboxylase	CSAD	Up-regulated	0.027375	0.428
Bt.12339.1.S1_at	Pyruvate Carboxylase	PC *	Down-regulated	0.03	-1.767
Bt.12553.1.S1_at	Haptoglobin	HP	Up-regulated	0	0.843
Bt.12768.1.S1_at	Phosphoenolpyruvate Carboxykinase 1	PCK1 *	Down-regulated	0.06	-1.996
Bt.13622.1.A1_at	N/A	LOC505099	Up-regulated	1.10E-05	0.837
Bt.16399.1.A1_at	Betaine--Homocysteine S-Methyltransferase	BHMT	Down-regulated	0	-0.993
Bt.17242.1.A1_at	Cytochrome P450, Family 2, Subfamily B, Polypeptide 6	CYP2B6	Down-regulated	0	-1.115
Bt.17368.1.A1_at	Purinergic Receptor P2Y, G-Protein Coupled, 14	P2RY14	Down-regulated	0.000881	-0.303
Bt.18083.1.S1_at	3-Hydroxyacyl-Coa Dehydratase 4	PTPLAD2	Down-regulated	0.026846	-0.525
Bt.2091.1.S1_at	Dna-Damage-Inducible Transcript 4	DDIT4	Down-regulated	0.015038	-0.480
Bt.20989.1.S1_at	Nicotinamide Nucleotide Adenylyltransferase 2	NMNAT2	Down-regulated	0	-0.568
Bt.21048.1.S1_at	Lim Domain Binding 3	LDB3	Down-regulated	0.000498	-0.638
Bt.21048.2.S1_at	Lim Domain Binding 3	LDB3	Down-regulated	1.00E-05	-0.640
Bt.2120.1.S1_at	Carboxypeptidase Q	CPQ	Down-regulated	0	-1.388
Bt.2120.2.S1_at	Carboxypeptidase Q	CPQ	Down-regulated	0	-1.465
Bt.21883.1.S1_at	Placenta-Specific 8	PLAC8	Up-regulated	0.001849	0.463
Bt.21997.1.S1_at	Protein Phosphatase, Mg2+/Mn2+ Dependent, 1K	PPM1K	Down-regulated	0.001242	-0.358
Bt.22629.1.A1_at	Chromosome 21 Open Reading Frame 62	C21orf62	Down-regulated	0.026846	-0.522
Bt.22867.2.A1_at	1	BOLA-DQA1	Down-regulated	0	-0.645
Bt.23093.1.S1_at	Chemokine (C-X-C Motif) Ligand 2	CXCL2	Down-regulated	0.002128	-0.445
Bt.23204.1.S1_at	Glutathione S-Transferase Theta 1	GSTT1	Up-regulated	0.011498	0.677
Bt.25669.1.S1_at	Mucolipin 2	MCOLN2	Up-regulated	0.00936	0.655
Bt.278.1.S1_at	Serum Amyloid A1	SAA1	Down-regulated	5.20E-05	-1.008
Bt.28208.1.S1_at	Fructose-1,6-Bisphosphatase 2	FBP2	Down-regulated	0.000881	-0.412
Bt.28278.1.S1_at	Angiotensin I Converting Enzyme 2	ACE2	Down-regulated	0.001676	-0.668
Bt.28521.1.S1_at	Annexin A13	ANXA13	Down-regulated	0	-1.140
Bt.28878.1.S1_at	Aspartoacylase	ASPA	Down-regulated	0	-1.503
Bt.29815.1.S1_x_at	Major Histocompatibility Complex, Class I, B	BOLA-B	Down-regulated	0	-1.597
Bt.350.1.S1_at	Histocompatibility Complex, Class Ii, Dq Beta, Type 1	BOLA-DQB1	Up-regulated	0	0.870
Bt.350.1.S1_x_at	Histocompatibility Complex, Class Ii, Dq Beta, Type 1	BOLA-DQB1	Up-regulated	0	0.738
Bt.3551.1.S1_at	Solute Carrier Family 17 (Vesicular Nucleotide Transporter), Member 9	SLC17A9	Up-regulated	9.00E-06	0.837

Bt.3809.1.S1_at	Lactate Dehydrogenase A	LDHA	Down-regulated	0.003635	-0.348
Bt.4169.1.A1_at	Conglutinin	CGN1	Up-regulated	0.028848	0.362
Bt.4404.1.A1_at	Protease, Serine, 2 (Trypsin 2)	PRSS2	Up-regulated	0	1.232
Bt.4594.1.S1_at	Histocompatibility Complex, Class Ii, Dq Beta, Type 1	BOLA-DQB1	Up-regulated	0	1.343
Bt.4751.1.S1_a_at	Major Histocompatibility Complex, Class Ii, Dq Alpha, Type 2	BOLA-DQA2	Up-regulated	0	1.447
Bt.4751.2.S1_a_at	Major Histocompatibility Complex, Class Ii, Dq Alpha, Type 2	BOLA-DQA2	Up-regulated	0.000311	0.752
Bt.4939.1.S1_at	Secreted Frizzled-Related Protein 2	SFRP2	Down-regulated	9.00E-06	-0.357
Bt.5037.1.S1_at	S100 Calcium-Binding Protein A10	S100A10	Down-regulated	0	-1.162
Bt.5037.1.S2_at	S100 Calcium-Binding Protein A10	S100A10	Down-regulated	0	-1.417
Bt.6800.1.A1_at	Rasgef Domain Family, Member 1B	RASGEF1B	Down-regulated	0.001035	-1.043
Bt.7190.1.S1_at	Cytochrome P450, Family 11, Subfamily A, Polypeptide 1	CYP11A1	Up-regulated	2.00E-06	0.922
Bt.7490.1.A1_at	Methylenetetrahydrofolate Dehydrogenase (Nadp+ Dependent) 1-Like	MTHFD1L	Down-regulated	8.00E-06	-0.623
Bt.9289.2.S1_at	Carnitine Palmitoyltransferase 1A *	CPT1A *	Down-regulated	0.08	-1.594

1. The P-values of the DEGs identified in the microarray were obtained from local-pooled-error (LPE) tests within time points, followed by a false-discovery rate control. The P-values of the DEGs identified in quantitative polymerase chain reactions (qPCRs) were obtained from repeated-measures ANOVA. 2. Log2-fold was calculated as that of the high-energy (HIGH) feeding group relative to the controlled-energy (CON) feeding group. 3. The genes marked with an asterisk (*) are from quantitative reverse transcriptase-polymerase chain reaction (qRT-PCR) analyses.

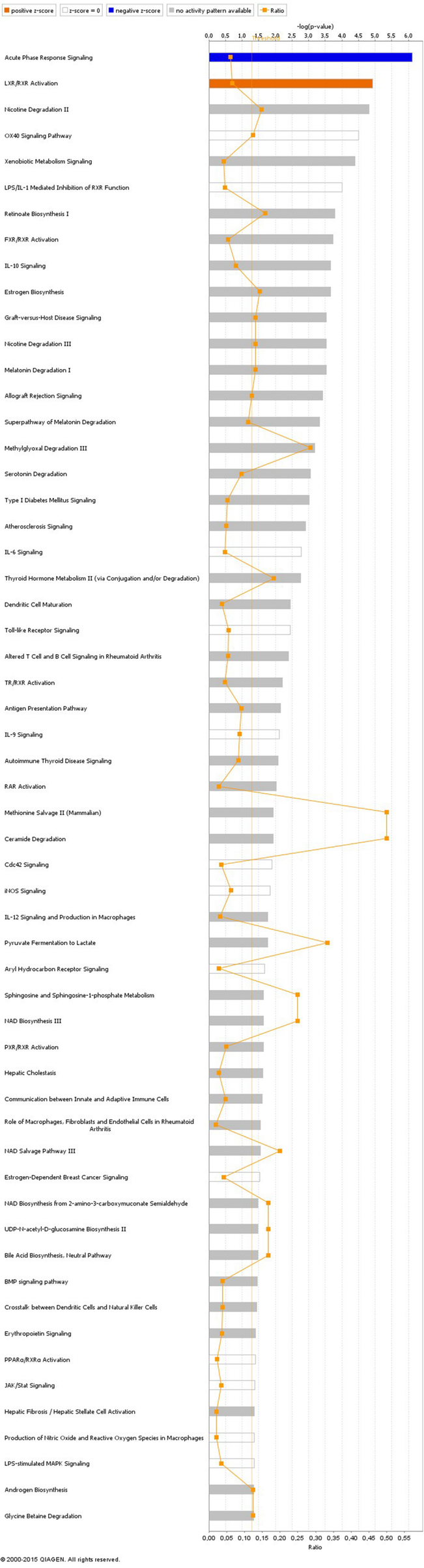

Supplemental Figure S1.

Summary of canonical pathway analyses in Ingenuity Pathway Analysis (IPA). The lengths of the bars indicate the probability of significant upregulation or downregulation of the pathways. Significant pathways were marked in color, with orange representing upregulation in the high-energy (HIGH) feeding group versus controlled-energy (CON) feeding group and blue representing downregulation in HIGH versus CON. The node on each bar indicates the ratio of the differentially expressed genes (DEGs) involved in the pathway in the dataset to the total number of genes involved in the pathway.

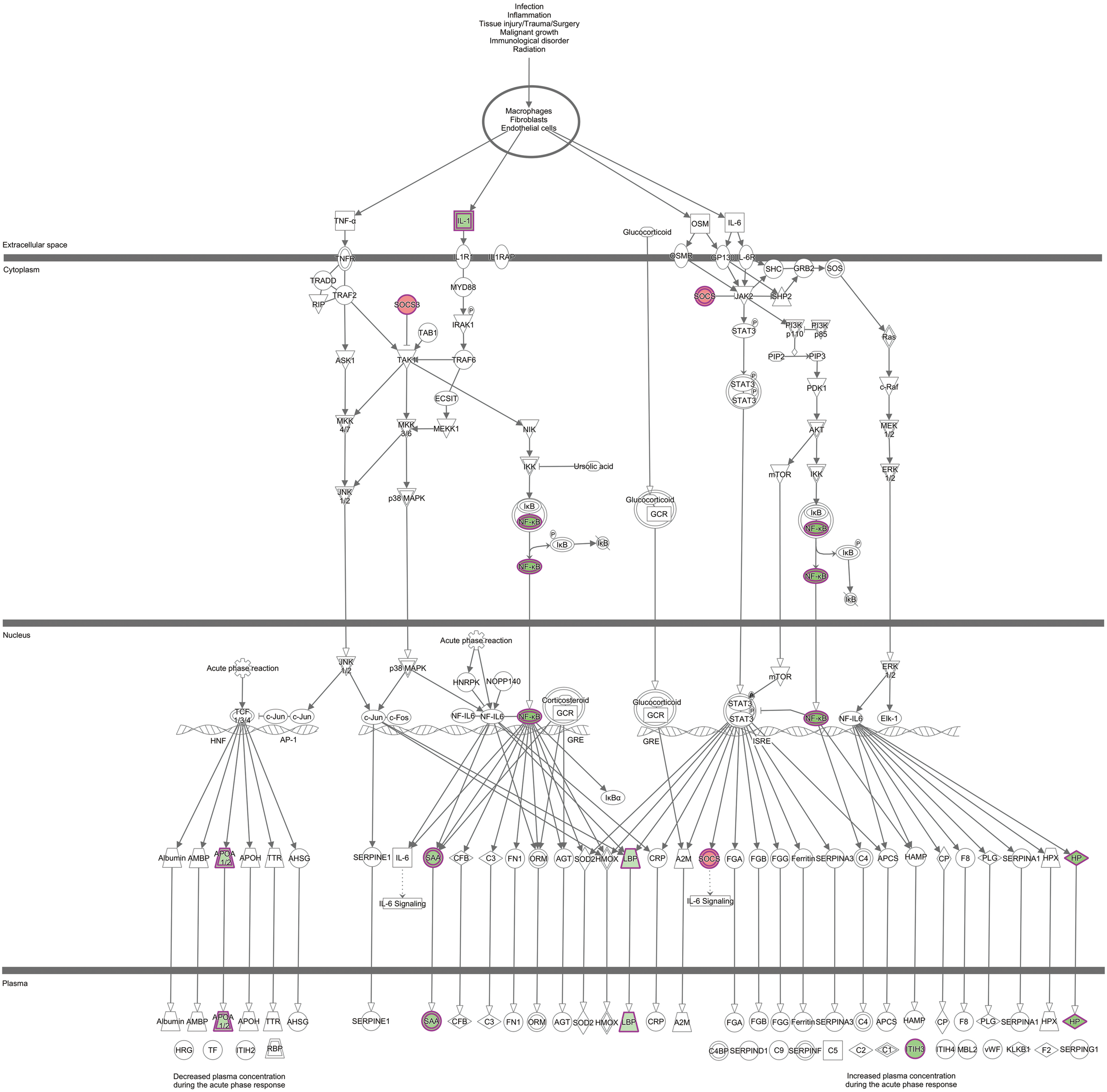

Supplemental Figure S2.

Acute phase response signaling pathway in Ingenuity Pathway Analysis (IPA). Differentially expressed genes (DEGs) in the dataset were marked in color, with red representing upregulation in the high-energy (HIGH) feeding group versus controlled-energy (CON) feeding group.

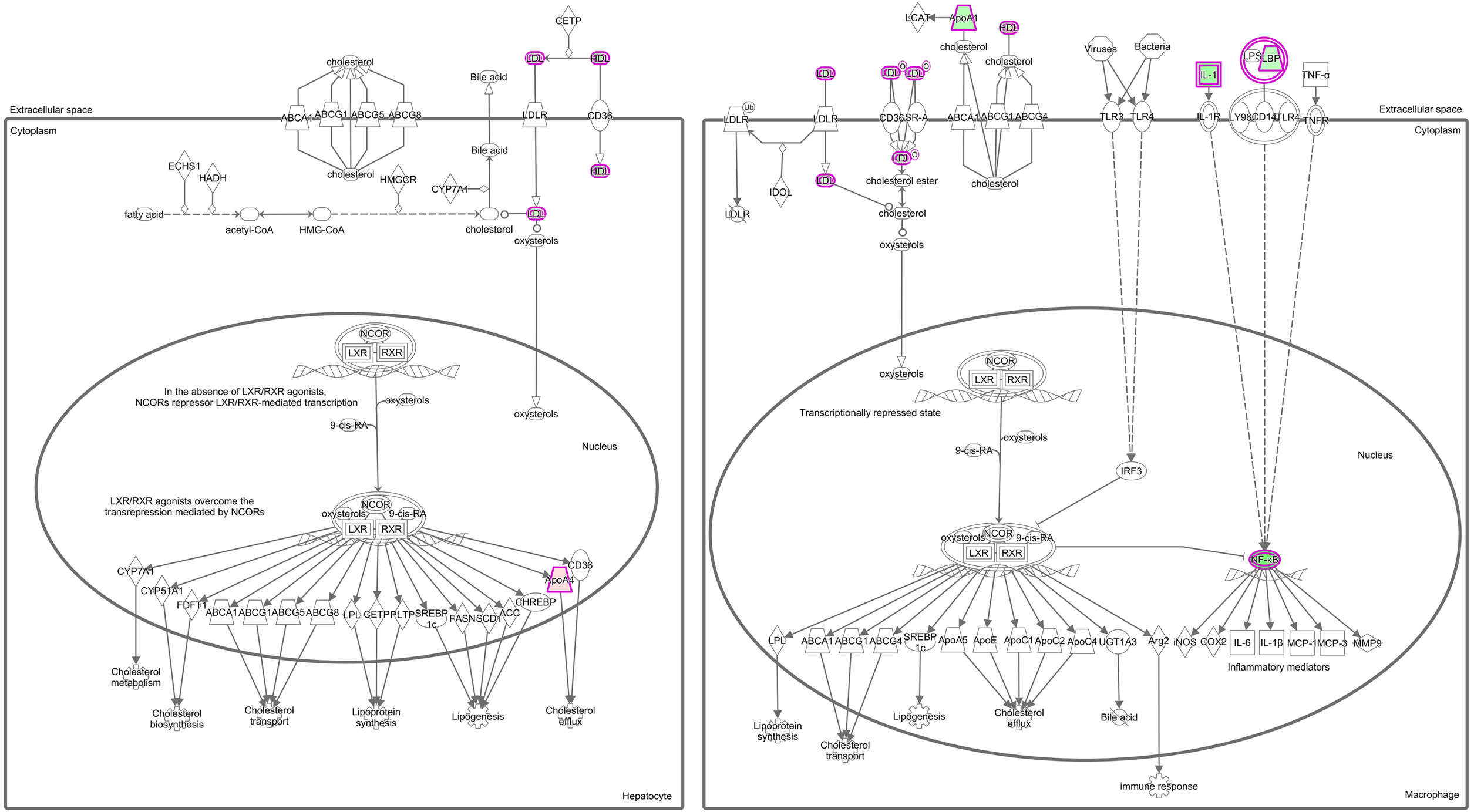

Supplemental Figure S3.
Liver X receptor/retinoid X receptor (*LXR/RXR*) activation pathway in Ingenuity Pathway Analysis (IPA). Differentially expressed genes (DEGs) in the dataset were marked in color, with red representing upregulation in the high-energy (HIGH) feeding group versus controlled-energy (CON) feeding group.

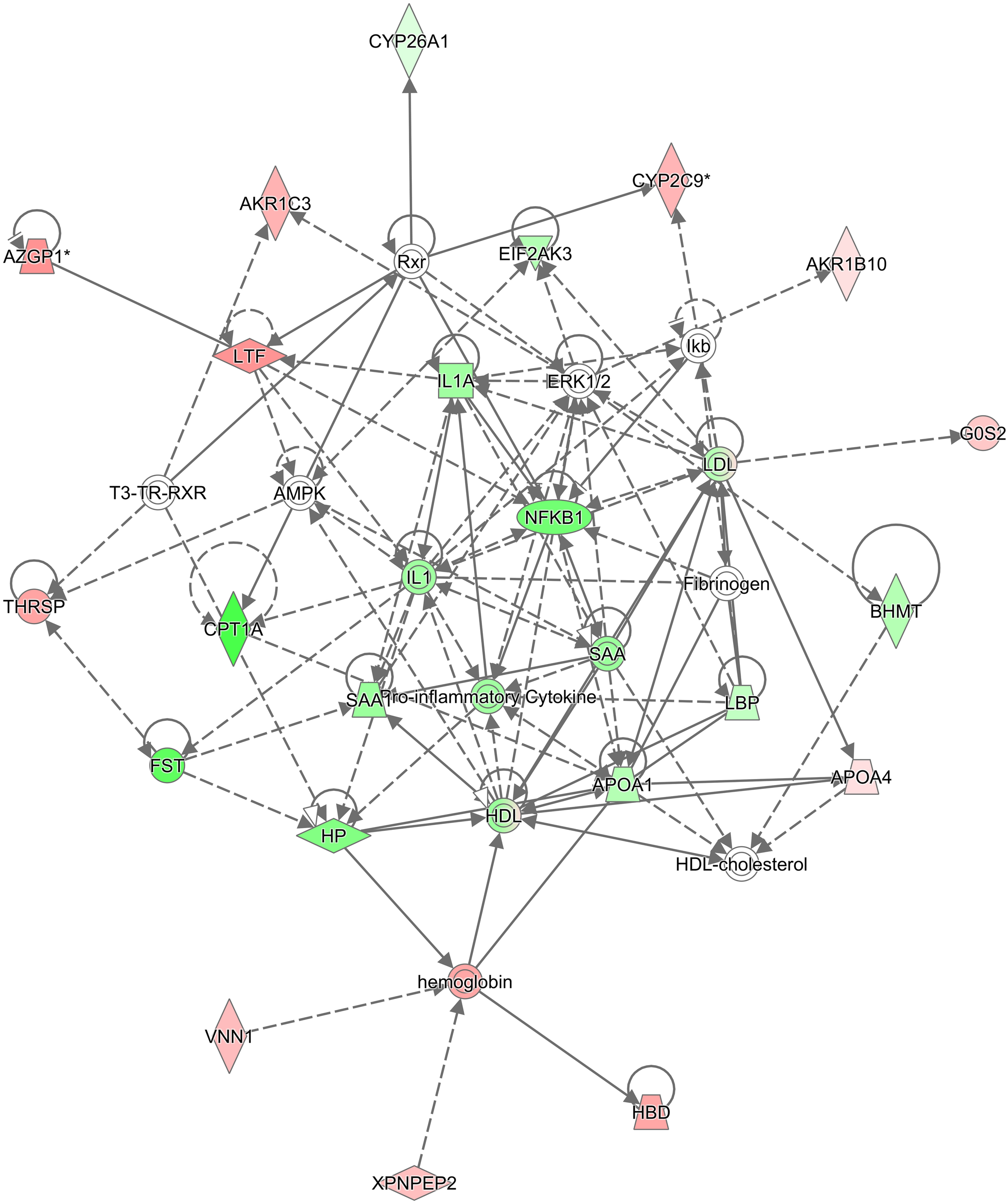

Supplemental Figure S4.

Network: lipid metabolism, small-molecule biochemistry, and vitamin and mineral metabolism. The network is displayed graphically as nodes (genes). The solid lines indicate direct interaction between genes. The dashed line indicates indirect interaction between genes. The node color intensity indicates the expression of genes, with red representing upregulation and green downregulation in the high-energy (HIGH) feeding group relative to the controlled-energy (CON) feeding group.